iScience

Article

Epigenetic control of myogenic identity of human muscle stem cells in Duchenne muscular dystrophy

Graphical abstract

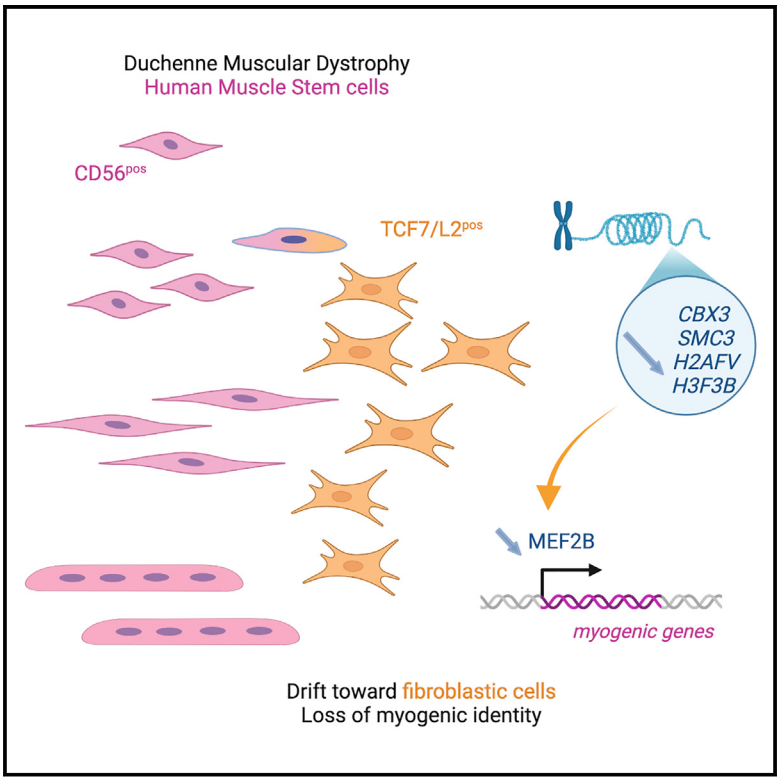

Highlights

- Duchenne muscular dystrophy muscle stem cells (DMD-MuSCs) exhibit unaltered myogenesis
- DMD-MuSCs loose myogenicity faster than normal cells due to epigenetic enzyme downexpression
- Re-expression of *CBX3*, *SMC3*, *H2AFV*, and *H3F3B* prevent the MuSC identity drift
- *MEF2B* transcription factor is key in the maintenance of myogenic identity in human MuSCs

Authors

Jimmy Massenet, Michèle Weiss-Gayet, Hina Bandukwala, ..., Cyril Gitiaux, F. Jeffrey Dilworth, Bénédicte Chazaud

Correspondence

fdilworth@wisc.edu (F.J.D.), benedicte.chazaud@inserm.fr (B.C.)

In brief

Epigenetics; Stem cells research; Integrative aspects of cell biology

Massenet et al., 2024, iScience *27*, 111350
December 20, 2024
https://doi.org/10.1016/j.isci.2024.111350

CellPress

iScience

CellPress
OPEN ACCESS

Article

Epigenetic control of myogenic identity of human muscle stem cells in Duchenne muscular dystrophy

Jimmy Massenet,[1,2] Michèle Weiss-Gayet,[1] Hina Bandukwala,[2] Wilhelm Bouchereau,[1] Stéphanie Gobert,[1] Mélanie Magnan,[3] Arnaud Hubas,[4] Patrick Nusbaum,[4] Isabelle Desguerre,[5,6] Cyril Gitiaux,[5,7] F. Jeffrey Dilworth,[2,8,9,*] and Bénédicte Chazaud[1,9,10,*]

[1]Institut NeuroMyoGène, Physiopathologie et Génétique du Neurone et du Muscle Université Claude Bernard Lyon 1, CNRS U5261, Inserm U1315, University Lyon, Lyon, France
[2]Sprott Center for Stem Cell Research, Regenerative Medicine Program, Ottawa Hospital Research Institute, Ottawa, ON, Canada
[3]Institut Cochin, Université Paris-Cité, Inserm U1016, CNRS UMR8104, Paris, France
[4]Hôpital Cochin – Port-Royal, Centre de Ressources Biologiques, Paris, France
[5]Centre de Référence des Maladies Neuromusculaires Nord/Est/Ile de France, AP-HP, Hôpital Necker Enfants Malades, Université Paris-Cité, Paris, France
[6]Université Paris Cité, IHU Imagine, 75015 Paris, France
[7]Service d'explorations Fonctionnelles, Unité de Neurophysiologie Clinique, AP-HP, Hôpital Necker Enfants Malades, Paris, France
[8]Department of Cell and Regenerative Biology, University of Wisconsin – Madison, Madison WI 53705, USA
[9]These authors contributed equally
[10]Lead contact
*Correspondence: fdilworth@wisc.edu (F.J.D.), benedicte.chazaud@inserm.fr (B.C.)
https://doi.org/10.1016/j.isci.2024.111350

SUMMARY

In Duchenne muscular dystrophy (DMD), muscle stem cells' (MuSCs) regenerative capacities are overwhelmed leading to fibrosis. Whether MuSCs have intrinsic defects or are disrupted by their environment is unclear. We investigated cell behavior and gene expression of MuSCs from DMD or healthy human muscles. Proliferation, differentiation, and fusion were unaltered in DMD-MuSCs, but with time, they lost their myogenic identity twice as fast as healthy MuSCs. The rapid drift toward a fibroblast-like cell identity was observed at the clonal level, and resulted from altered expression of epigenetic enzymes. Re-expression of *CBX3*, *SMC3*, *H2AFV*, and *H3F3B* prevented the MuSC identity drift. Among epigenetic changes, a closing of chromatin at the transcription factor *MEF2B* locus caused downregulation of its expression and loss of the myogenic fate. Re-expression of MEF2B in DMD-MuSCs restored their myogenic fate. MEF2B is key in the maintenance of myogenic identity in human MuSCs, which is altered in DMD.

INTRODUCTION

After an injury, adult skeletal muscle regenerates thanks to muscle stem cells (MuSCs) that operate adult myogenesis to ensure the formation of new myofibers while repopulating the pool of stem cells for further needs.[1] To execute myogenesis, MuSCs transit through sequential states including activation (exit from quiescence), proliferation (expansion), exit from the cell cycle and commitment into terminal myogenic differentiation, and eventually fusion into multinucleated myotubes and myofibers.[1] The characteristics of each cell fate are determined through specific epigenetic mechanisms that determine the subset of genes that are expressed, through the control of the accessibility of the transcriptional machinery to specific loci. The chromatin state allows the expression of the ad hoc genes in a spatiotemporal manner. Changes in chromatin organization are required for mediating decisions of cell fate and differentiation.[2] In response to environmental cues, chromatin organization is altered and modifies the accessibility of the transcription machinery to the gene sequences, which is modulated by several levels of regulation, at the DNA and histone levels. Huge efforts have been made to decipher the chromatin organization and the key epigenetic regulators that control adult myogenesis.[3–5] Investigations were mainly done in the context of regeneration of healthy muscle.

Epigenetic marks and chromatin dynamics are reversible and change according to the modifications of the environment of the cells. Such environmental changes are particularly important during muscular diseases, and particularly during degenerative myopathies, where attempts of muscle regeneration occur in an environment encompassing tissue damage, inflammation, and fibrosis. However, chromatin dynamic response to environmental changes and how it impacts of muscle regeneration has been poorly investigated in the context of muscular diseases. Duchenne muscular dystrophy (DMD) is caused by mutations in the dystrophin gene.[6–8] The absence of dystrophin causes sarcolemma fragility and costamere disorganization, leading to myofiber damage.[9,10] Patient muscles present asynchronous cycles of damage and regeneration and are characterized by a progressive loss of muscle tissue associated with chronic

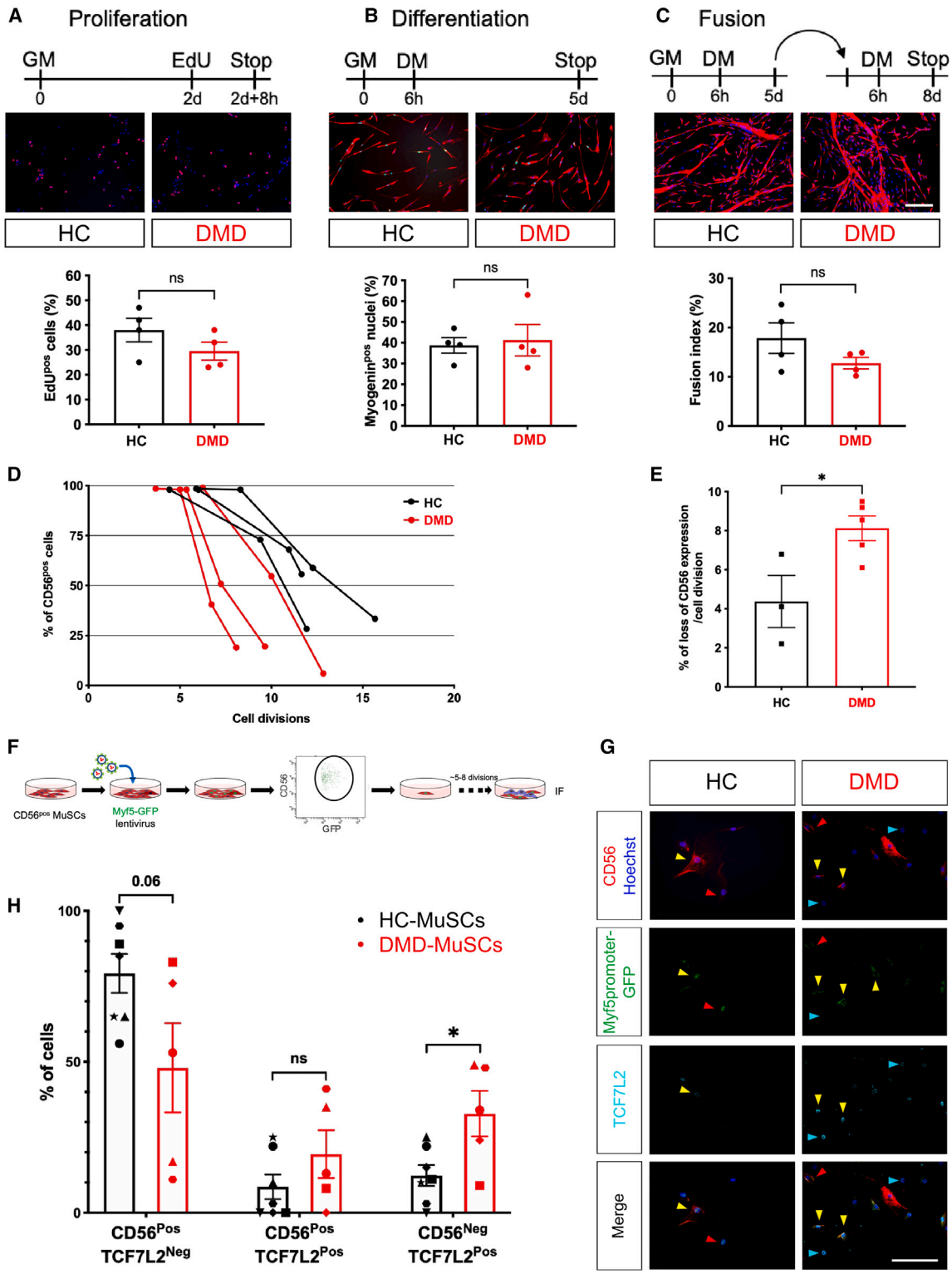

Figure 1. *In vitro* behavior of DMD-MuSCs

(A–C) CD56^{pos} MuSCs isolated from healthy control (HC) and Duchenne (DMD) muscles were analyzed for their capacity to implement *in vitro* myogenesis. (A) Proliferation was assessed in growth medium (GM) as the number of EdU^{pos} cells (red). (B) Differentiation was quantified after 5 days in differentiation medium

(legend continued on next page)

inflammation and fibrosis. The defect in muscle repair that is finally observed in DMD patients has been attributed to both MuSC cell-autonomous and non-autonomous mechanisms. Most of the investigations were done in the mdx mouse model of DMD, which poorly recapitulates the clinical features observed in DMD patient's muscle.[11,12] Studies reported intrinsic alterations of MuSC differentiation and self-renewal capacities[13,14] while others reported that the MuSC environment directly impacts on MuSC function.[15] Finally, lineage tracing experiments reported that in the mdx muscle, a portion (7%–20%) of MuSCs acquires a fibroblastic phenotype, suggesting strong alteration of chromatin organization in such converted cells in response to environmental cues.[16–18]

Given the difficulties to unravel the mechanisms of failure of muscle repair in DMD in the mdx model, using human DMD MuSCs is an attractive alternative. Pioneer investigations using cells isolated from human muscle biopsies led to contradictory results about the myogenic potential of cells issued from DMD muscle as compared with cells isolated from healthy muscle.[19–24] Discrepant results are likely due to the lack of efficient isolation procedure of human MuSCs at that time, leading to the analysis of mixed cultures containing various cell types. During the early 2000s, isolation techniques were developed, using FACS or magnetic cell sorting, allowing the enrichment of highly purified (more than 95%–98%) MuSCs. Those techniques were based on the expression of CD56 (or neural cell adhesion molecule [NCAM]) by MuSCs, expression which was established as a reliable marker of myogenicity of human MuSCs.[25–30]

In the present study, we examined the myogenic potential and the myogenic identity of human MuSCs isolated from DMD muscle as compared with healthy MuSCs. Being isolated at the time of diagnosis, DMD-MuSCs have been supposedly living over time with the constant presence of stressors around, which may impact the chromatin organization. We functionally investigated some features of chromatin alterations in DMD-MuSCs that may explain the rapid identity drift observed in these cells and we identified epigenetic regulators involved in the maintenance of the myogenic identity of human MuSCs.

RESULTS

Human MuSCs were obtained from the hospital cell bank as CD56^{pos} enriched cell populations (cells were previously expanded and sorted based on their CD56 expression [Figures S1A and S1B]). CD56 has been established as a reliable marker of myogenicity of human MuSCs.[25–30] Indeed, 100% of CD56^{pos} cells expressed the transcription factor Pax7 (Figure S1C). All 28 samples used in this study were highly enriched for CD56^{pos} MuSCs with an average purity of 92% for DMD and 96% for healthy control (HC) cells (Figure S1D).

CD56^{pos} DMD-MuSCs exhibit normal myogenic properties

CD56^{pos} MuSCs derived from DMD (DMD-MuSCs) and healthy control (HC-MuSCs) muscles were cultured to evaluate their capacity to perform *in vitro* myogenesis. Proliferation of CD56^{pos} cells cultured in growth medium, assessed by EdU incorporation, was similar in HC- and DMD-MuSCs (Figure 1A). Commitment into terminal myogenic differentiation of CD56^{pos} cells, assessed by their expression of myogenin when cultured in differentiation medium, was also not different in HC- and DMD-MuSCs (Figure 1B). Finally, a fusion assay of differentiated cells (myocytes) showed similar capacity of HC- and DMD-MuSCs to form myotubes (Figure 1C). These data show that the myogenic capacities were not altered in CD56^{pos} DMD-MuSCs.

DMD-MuSCs lose their myogenic identity twice as fast as HC-MuSCs

A progressive loss of CD56 expression has been described during the culture of human CD56^{pos} MuSCs issued from healthy muscle, preventing their use after 4–5 passages.[25,28,31,32] Starting from 100% CD56^{pos} HC- and DMD-MuSC populations, we found that the number of CD56^{pos} cells decreased with time in culture, as expected; however, this decrease occurred earlier and faster in DMD-MuSCs (Figure 1D). The rate of CD56^{pos} cells lost per cell division was calculated over a period of 10 population doublings and was found to be twice as high in DMD-MuSCs vs. HC-MuSCs (8.1 ± 0.6% vs. 4.4 ± 1.3% per cell division) (Figure 1E). The loss of CD56^{pos} cells could be due to either apoptosis of CD56^{pos} cells, overtake of CD56^{neg} cells in the culture (although being not more than 2% of the cells in the starting cultures), or cellular conversion of CD56^{pos} into CD56^{neg} cells. To investigate apoptosis, CD56^{pos} MuSCs were maintained in growth medium until about half of the cells have lost CD56 expression, then cells were sorted as CD56^{pos} and CD56^{neg} cell populations (Figure 2A) and were analyzed. Terminal deoxynucleotidyl transferase dUTP nick end labeling (TUNEL) assay indicated that both CD56^{pos} and CD56^{neg} cells from HC and DMD donors showed very low rates of apoptosis (from 1.7% to 3.3% of the cultured cells) (Figure S1F), ruling out apoptosis as a mechanism for CD56 loss in MuSC population. We then used cells from adult healthy samples to compare the growth rate and CD56 expression of 100% CD56^{pos} cells,

(DM) as the number of myogenin^{pos} cells (green) among desmin^{pos} cells (red). (C) Fusion index was quantified in differentiated cells grown at high density, as the number of nuclei in desmin expressing myotubes (red) related to the total number of nuclei. Hoechst labels nuclei (blue). Bar: 100 μm.

(D) Expression of CD56 was evaluated by flow cytometry during the culture of initially pure CD56^{pos} HC- and DMD-MuSCs in growth medium.

(E) Calculation of the loss of CD56 per cell division from (D).

(F) Experimental procedure of the clonal culture of Myf5-transduced CD56^{pos} MuSCs.

(G) Immunostaining of clones for CD56 (red), GFP(Myf5) (green) and TCF7L2 (cyan). Hoechst labels nuclei (blue). Red arrowheads show myogenic CD56^{pos}Myf5^{pos} cells, blue arrowheads show fibrogenic TCF7L2^{pos} cells and yellow arrowheads show cells harboring both myogenic and fibrogenic markers. Bar: 50 μm.

(H) Quantification of cells according to the immunostaining shown in (G). Each shape symbol represents one clone. Results are means ± SEM of 3–9 samples in (A–E) and of 6 clones issued from 3 HC donors and of 5 clones issued from 3 DMD donors in (H). ns: non significant, *$p < 0.05$ using unpaired (A–E) or paired (H) t test.

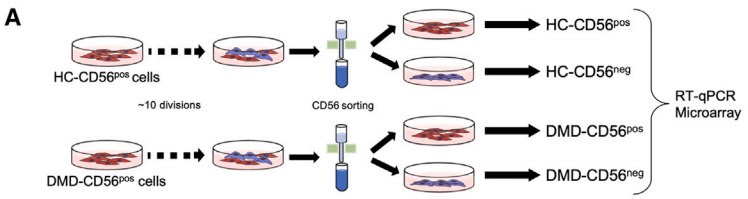

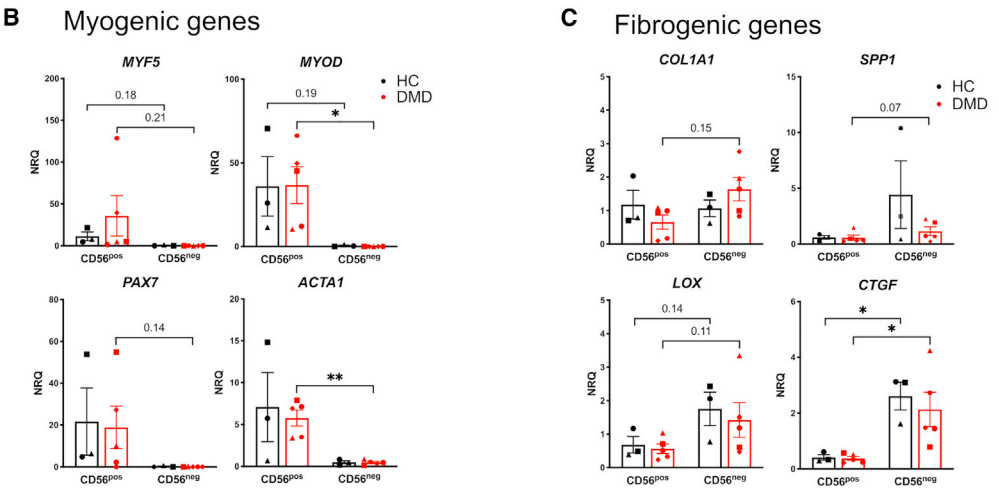

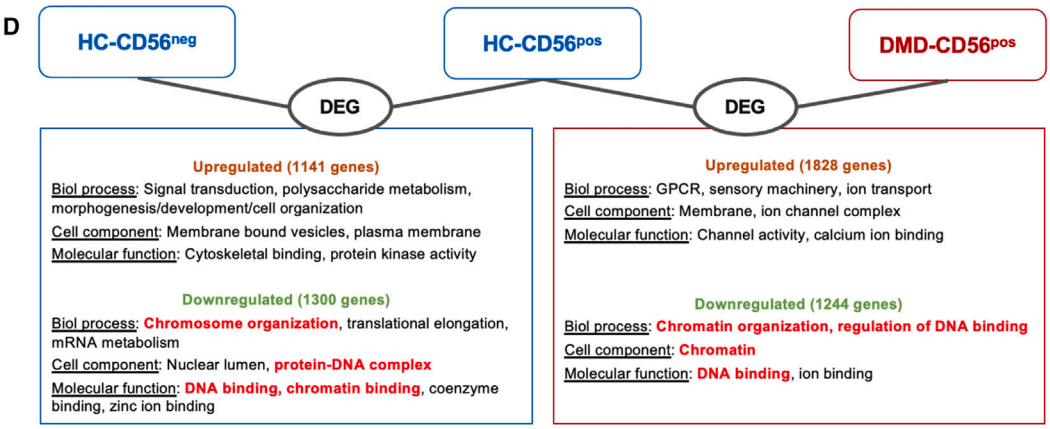

E Microarray values of candidate genes

Candidate genes	HC-CD56neg vs. HC-CD56pos		DMD-CD56pos vs. HC-CD56pos	
	p-value	fold change	p-value	fold change
CBX1	0.027	-1.32	0.020	-1.54
CBX3	0.033	-1.45	0.049	-1.51
CTCF	0.002	-1.36	0.004	-1.41
H2AZ2	0.003	-2.69	0.050	-2.09
H3F3B	0.041	-1.25	0.007	-1.47
ING3	0.003	-1.28	0.035	-1.22
MSL3	0.013	-1.25	0.042	-2.02
SETDB1	0.040	-1.39	0.001	-1.38
SMARCA2	0.002	-1.53	0.037	-1.37
SMC3	0.047	-1.23	0.023	-1.34
SUPT3H	0.018	-1.52	0.007	-1.35

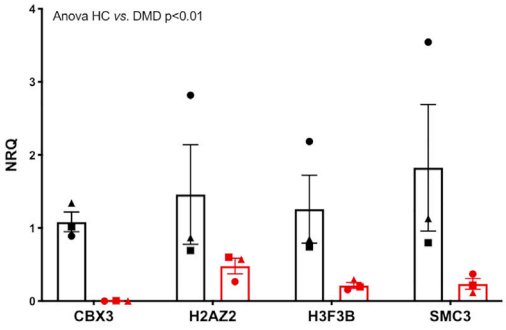

(legend on next page)

100% CD56^{neg} cells and a mixed culture of 50:50 CD56^{pos}:CD56^{neg} cells. Both growth rate and loss of CD56 expression did not differ between the 3 conditions (Figures S1G and S1H), indicating that the presence of CD56^{neg} cells in the culture did not impact on CD56^{pos} cell behavior, and ruling out a faster expansion of CD56^{neg} cells to explain the CD56 loss in MuSC cultures.

To further investigate the conversion of CD56^{pos} cells into CD56^{neg} cells, we performed clonal cell cultures. CD56^{pos} cells from HC and DMD donors were transduced with lentiviruses encoding GFP under the control of the *Myf5* promoter region to fluorescently label cells capable of expressing this myogenic marker. Double CD56^{pos}/GFP^{pos} cells were sorted by fluorescence-activated cell sorting (FACS) as single cells and seeded in 96-well plates (Figure 1F). Examination of each well confirmed the presence of only a single CD56^{pos}/GFP^{pos} cell (Figure S1E), providing strong evidence that we were starting with a single myogenic cell. Clones were grown for 4 to 6 weeks in proliferating medium, then immunostained for CD56 and TCF7L2, a transcription factor expressed by human muscle fibroblasts and fibroadipogenic precursors[33,34] (Figure 1G). Clones derived from DMD-MuSCs gave rise to 40% less CD56^{pos}/TCF7L2^{neg} cells than those derived from HC-MuSCs (48% vs. 79%) and they produced 2.6-fold more CD56^{neg}/TCF7L2^{pos} cells (33% vs. 13%) (Figure 1H). Double-positive cells were observed in both HC and DMD cultures, possibly representing an intermediate status (Figure 1H). These results show at the cellular level the conversion of CD56^{pos} MuSCs into CD56^{neg}/TCF7L2^{pos} cells, which was higher in DMD than in HC cultures.

To analyze the nature of the cells at the transcriptomic level, CD56^{pos} HC- and DMD-MuSCs were cultured until about 50% of the cells have lost CD56 expression, and cells were further sorted to obtained CD56^{pos} and CD56^{neg} populations issued from the same initial MuSCs (hereafter referred as HC-CD56^{pos}, HC-CD56^{neg}, DMD-CD56^{pos}, and DMD-CD56^{neg}) (Figure 2A). RT-qPCR experiments showed a dramatic decrease of the expression of the muscle-specific genes *PAX7*, *MYOD*, *MYF5*, and *ACTA1* genes in both HC- and DMD-CD56^{neg} cells, confirming the loss of myogenicity of these cells (Figure 2B). Inversely, the expression of genes associated with fibrogenesis, *COL1A1*, *CTGF*, *LOX*, and *SPP1*, was increased in CD56^{neg} cells (Figure 2C). No difference was observed between HC- and DMD-derived cells meaning that both HC- and DMD-MuSCs have a propensity to lose their myogenicity and acquire fibrogenic markers *in vitro* with time. However, our kinetic studies, as well as our clonal experiments, show that MuSCs from DMD muscle lose their myogenicity to acquire fibrogenic-like features faster than cells issued from normal muscle.

Reduced expression of epigenetic regulatory factors accompanies the loss of myogenicity in HC-CD56^{neg} cells and characterizes DMD-CD56^{pos} cells

We performed transcriptomic analysis on the four populations (HC-CD56^{pos}, HC-CD56^{neg}, DMD-CD56^{pos}, and DMD-CD56^{neg} as described in Figure 2A) using several comparisons. Gene ontology analysis of differentially expressed genes (Table S1) between CD56^{neg} and CD56^{pos} cells in both HC and DMD samples showed a common downregulation of genes involved in muscle function and an overexpression of genes involved in extracellular matrix (ECM) (Figure S2, "common in HC and DMD"), in accordance with the aforementioned RT-qPCR and IF analyses. Downregulated genes in HC-CD56^{neg} vs. HC-CD56^{pos} cells, that identified genes which expression was reduced at the time of the loss of myogenicity in normal cells, were related to chromatin organization, protein-DNA complex and DNA and chromatin binding (Figure 2D, red label in the left box). When comparing DMD-CD56^{pos} vs. HC-CD56^{pos}, to identify genes that were differentially expressed in DMD vs. HC myogenic cells, we observed that the downregulated genes were also related to chromatin organization, regulation of DNA binding, and chromatin (Figure 2D, red label in the right box). Scrutinizing those two lists of downregulated genes, 11 common genes were found (Figure 2E). RT-qPCR experiments run on HC-CD56^{pos} and DMD-CD56^{pos} cells confirmed the differential expression of 4 of them. They included: *CBX3* (encoding for the heterochromatin protein HP1γ), *H2AZ2* and *H3F3B* (encoding for H3.3), two histone variants, and *SMC3*, a subunit of the chromatin cohesion complex (Figure 2F).

These results indicate that the expression of 4 epigenetic regulators was decreased at the time of the myogenic loss in healthy MuSCs, and was already low in myogenic DMD-MuSCs, as compared with HC MuSCs.

Lentiviral expression of *CBX3*, *H2AZ2*, *H3F3B*, and *SMC3* rescues the myogenic potential of DMD-CD56^{pos} cells

The rate at which MuSCs lose their myogenicity (CD56 expression) is highly variable between patients, a result that has previously been reported for MuSCs from healthy donors.[31] To account for this variability between samples, the next experiments compared the same cell populations under various treatment conditions. In order to reexpress the 4 genes *CBX3*, *H2AZ2*, *H3F3B*, and *SMC3* in DMD-MuSCs, a protocol of exogenous expression of the 4 genes with a hemagglutinin (HA) reporter sequence using lentiviral transduction was designed (Figure 3A). The EF1a promoter was selected to ensure a stable long-term expression of

Figure 2. Gene expression in CD56^{pos} and CD56^{neg} cells from HC- and DMD-MuSC cultures

(A) Experimental procedure for CD56^{pos} and CD56^{neg} cell purification originating from pure healthy control (HC)- and Duchenne (DMD) CD56^{pos} population. Cells were cultured in growth medium.

(B and C) Normalized relative quantity (NRQ) expression by CD56^{pos} and CD56^{neg} cells from HC- and DMD-samples evaluated by RT-qPCR of (B) the myogenic related genes *PAX7*, *ACTA1*, *MYF5*, and *MYOD* and (C) the fibrogenic related genes *COL1A1*, *CTGF*, *LOX*, and *SPP1*. Results are means ± SEM of 3–6 samples. Each shape symbol represents cells issued from one initial culture.

(D) Gene ontology (DAVID software) of differentially expressed genes (DEG) after microarray analysis of CD56^{pos} and CD56^{neg} cells issues from healthy control (HC)- and Duchenne (DMD) CD56^{pos} MuSC cultures.

(E) Microarray fold change of the 11 genes found down expressed in both HC-CD56^{neg} vs. HC-CD56^{pos} and DMD-CD56^{pos} vs. HC-CD56^{pos} cells.

(F) NRQ expression by RT-qPCR of *CBX3*, *H2AZ2*, *H3F3B*, and *SMC3* genes in HC- and DMD-CD56^{pos} cells. Results from 3 HC and 3 DMD samples. Each shape symbol represents the same culture. $^{*}p < 0.05$, $^{**}p < 0.001$ using paired t test.

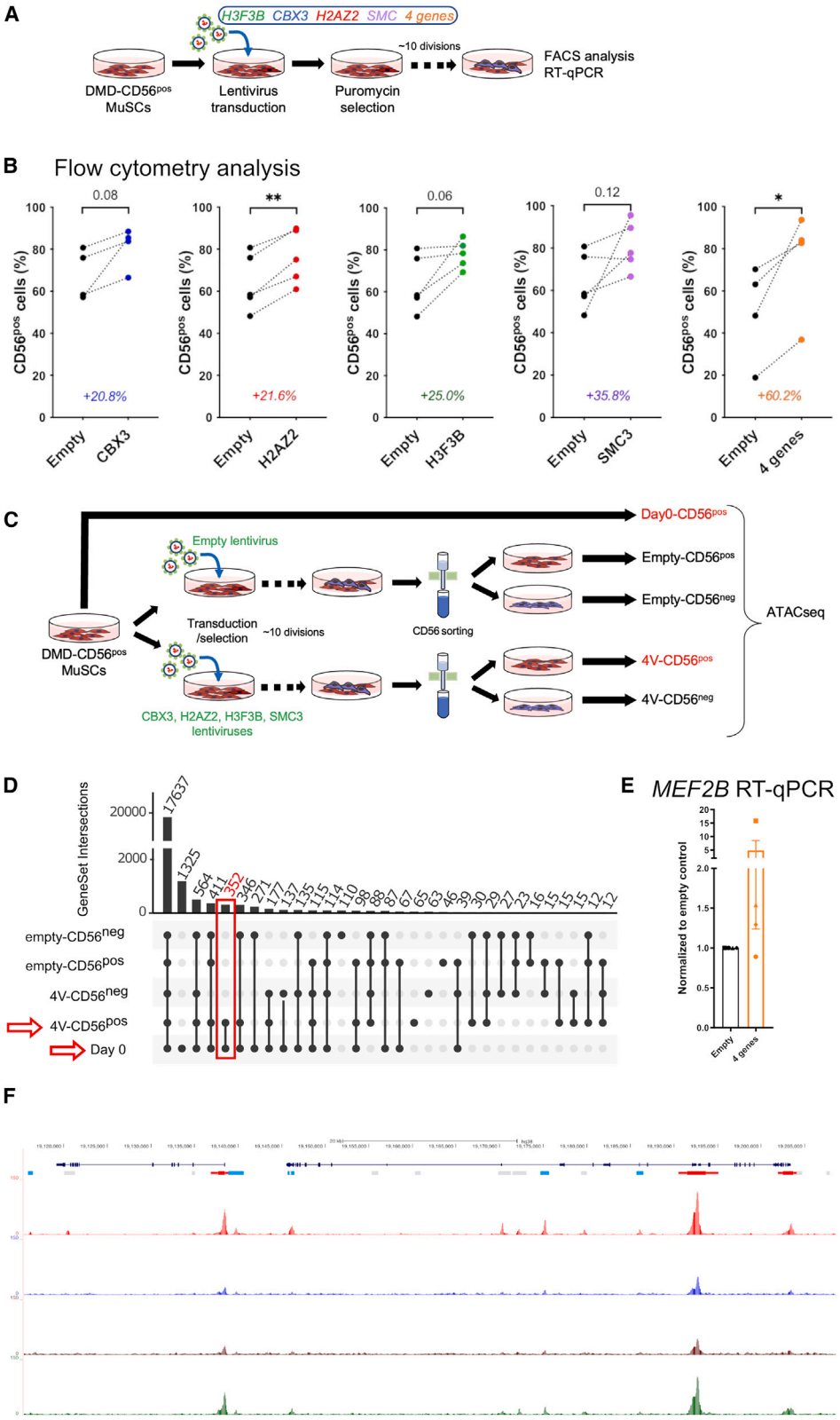

(legend on next page)

the transduced genes.[35] After transduction, cells were selected with puromycin and were cultured for 5–10 population doublings (i.e., the time for having around 50% loss of CD56 expression in DMD-MuSCs) before analysis. Immunostaining for HA confirmed the expression of the lentiviruses in MuSCs in all conditions but the control (Figure S3A). The expression of the 4 genes was evaluated by RT-qPCR and showed a robust increase of their expression, albeit some high variations were observed between some samples (Figure S3B). The expression of the *CBX3*, *H2AZ2*, *H3F3B*, and *SMC3* or of the 4 genes together in DMD-MuSCs was associated with an increase of the number of cells expressing CD56 after several weeks in culture as compared with cells transfected with an empty virus (Figure 3B). The mean increase of CD56 expression ranged from 20% to 35%. Additionally, the simultaneous transduction of DMD-CD56^{pos} cells with the 4 genes together induced a higher increase in the number of CD56^{pos} cells, of about 60%, as compared with the control (Figure 3B). Then, the capacity of the transduced cells to implement myogenesis was evaluated. Consistent with their increased ability to maintain CD56 expression, DMD-CD56^{pos} cells transduced with the 4 genes showed increased expression of *CD56*, *MYOD*, and *PAX7* mRNAs (Figure S3C). Due to the scarcity of the material, differentiation assays were limited to examining myogenin expression by immunofluorescence. In these conditions, we observed that DMD-CD56^{pos} cells transduced with the 4 genes were better able to maintain a capacity for differentiation into myogenin-expressing cells (Figure S3D). These results show that the re-expression of *CBX3*, *H2AZ2*, *H3F3B*, and *SMC3* genes in DMD-MuSCs counteracted the loss of CD56 expression and maintained their myogenic identity *in vitro*.

ATAC-seq identifies a target of CBX3, H2AZ2, H3.3, and SMC3 in MuSCs

To identify potential targets of CBX3, H2A.Z2, H3.3, and SMC3 in MuSCs, Assay for Transposase-Accessible Chromatin-sequencing (ATAC-seq) was performed before and after lentiviral transduction. Five conditions were analyzed (Figure 3C): (1) pure DMD-CD56^{pos} cells harvested before the infection (day 0); (2) empty-CD56^{pos} and (3) empty-CD56^{neg} cells resulting from DMD-CD56^{pos} cells transfected with empty lentivirus and cultured for about 10 population doublings; (4) 4V-CD56^{pos} and (5) 4V-CD56^{neg} cells resulting from DMD-CD56^{pos} cells transfected with *CBX3*, *H2AZ2*, *H3F3B*, and *SMC3* lentiviruses and cultured for 10 population doublings.

Prior loss of CD56, the exogenous expression of CBX3, H2AZ2, H3.3, and SMC3 proteins in DMD-CD56^{pos} cells broadly alters chromatin structure by promoting an increase and decrease accessibility at different positions across the genome (Figure S4A). Interestingly, at the transcription start sites of all genes, these proteins main function is to maintain an open chromatin accessibility (Figure S4B). It is the case in particular for myogenic related genes as *ITGA7*, while for fibrogenic related genes such as *SPP1*, the chromatin accessibility is decreased as compared to empty-CD56^{neg} DMD cells (Figure S4C).

Each ATAC-seq peaks obtained from the five conditions were associated to the unique closest gene to obtain a list of genes. Next, gene list comparison was performed to obtain a list of genes that were present in both day 0 and 4V-CD56^{pos} samples but that were absent in empty-CD56^{pos}, empty-CD56^{neg}, and 4V-CD56^{neg} samples (red arrows in Figure 3D). These 352 genes supposedly presented DNA sequences with open chromatin in both DMD-CD56^{pos} cells before the loss of CD56 and in cultured 4V-CD56^{pos} cells when accessibility was maintained thanks to the exogenous expression of CBX3, H2AZ2, H3.3, and SMC3 proteins. This list was cross-analyzed with the list of downregulated genes between DMD-CD56^{neg} and HC-CD56^{pos} cells identified by transcriptomics (Table S2). This resulted in a list of 78 genes defined as downregulated in DMD-CD56^{pos} cells and potential targets of CBX3, H2A.Z2, H3.3, and SMC3 in the ATAC-seq analysis (Figure S4D). Among them, only 34 genes presented an ATAC-seq peak at a regulatory sequence (Figure S4D). This list of 34 genes was refined by cross-analysis with ENCODE polyA-RNA-seq from normal human primary myoblasts (ENCSR000CWN) and allowed to retrieve 8 candidates: *ABHD14A*, *APBA3*, *EXOSC10*, *IF172*, *MEF2B*, *MIOS*, *NMP3*, and *TNKS* (Figure S4D). The expression of the 8 genes was evaluated by RT-qPCR in DMD-MuSCs after lentiviral transduction of *CBX3*, *H2AZ2*, *H3F3B*, *SMC3*, and of the 4 genes together (Figure S4E). Only *MEF2B* showed a robust increased expression in all conditions (Figures 3E and S4E), which was confirmed by an increase in chromatin accessibility at the *MEF2B* locus observed by an higher ATAC-seq peak intensity after the lentiviral transduction of all 4 genes together in DMD-MuSCs (Figure 3F).

MEF2B is a target of H2AZ2 and H3.3 in MuSCs and is required for the maintenance of the myogenic identity

To confirm that MEF2B was a target of CBX3, H2AZ2, H3.3, and SMC3, Cut&Tag technology was used to evaluate protein binding at the locus after lentiviral transduction of DMD-CD56^{pos} cells with lentiviruses expressing the 4 genes (Figure 4A). Results showed the presence of the H2AZ2 histone variant at the

Figure 3. Transduction of DMD-CD56^{pos} cells with CBX3, H2AZ2, H3F3B, and SMC3 coding lentiviruses

(A) Experimental procedure for DMD-CD56^{pos} cell transduction with lentiviruses. Cells were cultured in growth medium.

(B) Flow cytometry quantification of the number of CD56^{pos} cells in each condition. Results are from 4 to 5 DMD samples. Results are means ± SEM of 3 DMD samples (each shape symbol is used for cells issued from the same initial culture). *$p < 0.05$, **$p < 0.001$ using paired t test.

(C) Experimental design of ATAC-seq analysis of DMD-CD56^{pos} and DMD-CD56^{neg} cells initially non-transduced (day0-CD56^{pos}) or transduced with either empty (empty-CD56$^{pos/neg}$) or CBX3, H2AZ2, H3F3B, and SMC3 lentiviruses together (4V-CD56$^{pos/neg}$).

(D) UpSet plot of the comparison between the samples to identify genes differentially expressed in cells transduced with the 4 epigenetic regulators and non-transduced (red arrows) versus the 3 other conditions (red rectangle).

(E) Expression by RT-qPCR of the *MEF2B* gene in DMD-CD56^{pos} cells transduced with *CBX3*, *H2AZ2*, *H3F3B*, and/or *SMC3* lentiviruses.

(F) Screenshot of *MEF2B* locus. From top to bottom: chromosome scale, gene and regulatory sequences, ATAC-seq tracks in CD56^{pos} DMD-MuSCs initially non-transduced (red), DMD-CD56^{pos} (blue) and DMD-CD56^{neg} (brown) cells from CD56^{pos} DMD-MuSCs initially transduced with an empty vector, and DMD-CD56^{pos} cells from CD56^{pos} DMD-MuSCs initially transduced with the 4 epigenetic regulators (green). Results are means ± SEM of 4 samples.

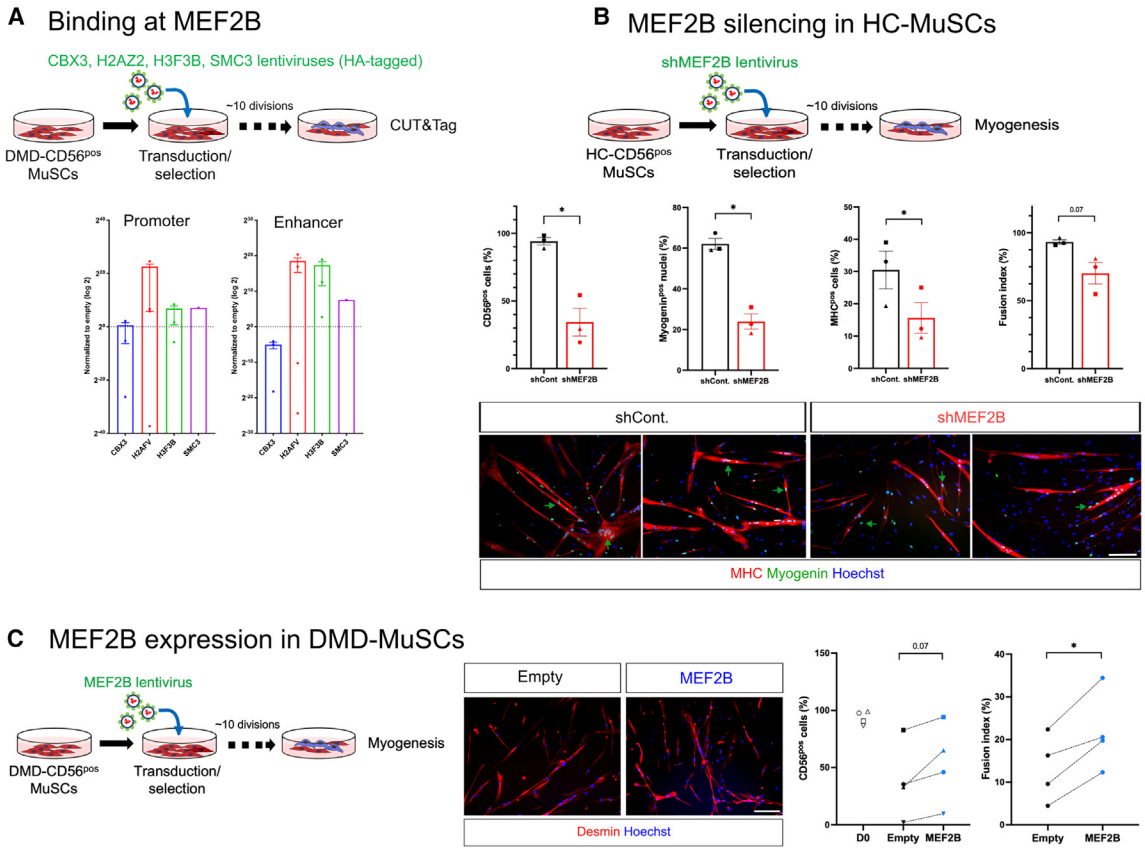

Figure 4. MEF2B and the maintenance of MuSC myogenicity

(A) Normalized relative quantity (NRQ) expression of *MEF2B* promoter and enhancer sequences by RT-qPCR after Cut&Tag library preparation with transduced DMD-CD56^{pos} cells using anti-HA antibodies to target the 4 epigenetic regulators. Dotted lines correspond to the expression after using control IgGs.

(B) Loss of function experiments where HC-CD56^{pos} were transduced with shRNA*MEF2B* lentiviruses (and shLuciferase as a control) and were analyzed for their CD56 expression by flow cytometry (far left) in growing medium, their expression of myogenin (left), the number of cells expressing MHC (right) and the fusion index (far right) after cultured in differentiation medium. Representative pictures of 2 cultures are shown for myogenin expression (green) and MHC expression (red) (blue = Hoechst).

(C) Gain of function experiments where DMD-CD56^{pos} cells were transduced with a lentivirus encoding for *MEF2B* and were analyzed for their CD56 expression by flow cytometry (left panel) in growing medium and for their myogenic capacity, assessed by their fusion index when cultured in differentiation medium. Representative pictures are shown for desmin (red) (blue = Hoechst). Data are shown for 4 DMD donors. *$p < 0.05$, using paired t test. Data are means ± SEM of 3 experiments. Each shape symbol represents the same culture. *$p < 0.05$ using paired t test. Bars: 100 μm.

promoter of the *MEF2B* gene (Figure 4A) and the presence of both H2AZ2 and H3.3 histone variants at the enhancer of the *MEF2B* gene (Figure 4A).

To further explore the function of MEF2B in the maintenance of the myogenic identity of CD56^{pos} cells, we performed loss and gain of function experiments. Short hairpin RNA (shRNA) lentivirus against *MEF2B* was transduced in HC-CD56^{pos} cells and the percentage of CD56^{pos} cells was evaluated after 10 population doubling following the puromycin selection (efficacy of the shRNAs on MEF2B expression is shown in Figure S4F). *MEF2B* knockdown using 4 different shRNAs resulted in a 50%–80% (average 64%) decrease in the percentage of CD56^{pos} cells as compared with the control shRNA (Figure 4B). Functionally, the myogenesis assay showed that the percentage of myogenin^{pos} nuclei and MHC^{pos} (myosin heavy chain) cells were strongly reduced in sh*MEF2B* treated HC-MuSCs (61% and 49%, respectively), and that the fusion capacity was also reduced by 25% in cells depleted of MEF2B (Figure 4B). Gain of function experiments included the transduction of DMD-CD56^{pos} cells with a *MEF2B* lentivirus as described previously for the 4 epigenetic regulators. The increase of *MEF2B* expression by transduced DMD-MuSCs (Figure S4F) was associated with an increase of the number of cells that expressed CD56 (+142%) (Figure 4C). Functionally, the DMD-MuSCs expressing *MEF2B* showed an increased capacity to differentiate and to form myotubes *in vitro* (+165%) (Figure 4C). Although cells from DMD patients exhibited highly variable loss of CD56 expression after about 10 cell divisions used to expand the transduced cells, we observed that cells from all 4 patients tested showed an improved ability to maintain their myogenicity when expressing exogenous MEF2B (Figure 4C). These results show that in DMD cells, alterations in the chromatin organization prevented the expression of *MEF2B* and that MEF2B was involved in the maintenance of the myogenic identity of MuSCs.

DISCUSSION

In the present study, we have examined how the DMD pathology affects the lineage fidelity of MuSCs. We found that human MuSCs isolated from DMD muscle continue to show myogenic properties that allow them to self-renew and differentiate to form new myofibers. Nevertheless, the overall MuSC population showed a rapid decline in their myogenicity where they drifted toward a fibroblast-like cell identity. This change in cell identity was observed at the clonal level, and resulted from the altered expression of epigenetic enzymes required to maintain the myogenic cell fate. Among the epigenetic changes, a closing of chromatin at the gene encoding the transcription factor MEF2B caused a downregulation of its expression, and a loss of the myogenic fate. Thus, our work identified MEF2B as a key mediator of the myogenic fate in human MuSCs.

The continued expansion of both healthy and DMD human MuSCs resulted in a loss of the myogenic identity in favor of a more fibroblast-like identity. Differential analysis of gene expression identified 4 important epigenetic factors (CBX3, H2A.Z2, H3.3, and SMC3) as being downregulated during the same time frame, suggesting that an epigenetic drift may be at the heart of this loss of myogenicity. The downregulation of each of these 4 factors is likely to contribute to the loss of myogenic gene expression. The SMC3 protein is a subunit of the cohesion complex, a key mediator of DNA looping that allows the communication between transcriptional enhancers and promoters to facilitate transcription.[36,37] In the absence of SMC3, a loss of topological associated domains (TADs) in the DMD-MuSCs would prevent the muscle-specific enhancers from communicating with promoters, and would result in a reduction of muscle gene expression. Similarly, CBX3 is required to maintain high levels of muscle gene expression as the euchromatin-associated protein helps facilitate transcriptional elongation by promoting RNA polymerase II pause-release and recruitment of the facilitates chromatin transcription (FACT) complex required for removal of nucleosomes that impede polymerase progression.[38–41] Finally, the histone variants H2A.Z2 and H3.3 proteins promote a transcriptionally permissive chromatin state by establishing a less stable nucleosome that is easily displaced by chromatin remodeling factors to establish open chromatin.[42–44] Interestingly, H3.3 been shown to contribute to cellular memory where methylation of the histone variant at the K4 position allowed reprogrammed cells to "remember" their myogenic cell identity.[45,46] H3.3 plays a dual role in maintaining cell memory by both promoting the muscle gene regulatory program and suppressing genes of alternate lineages. Indeed, when H3.3 is not incorporated into the genome due to loss of its chaperon protein HIRA, MuSCs begin to express non-muscle genes that are normally restricted to alternate lineages.[47] Thus, the loss of myogenicity observed due to the continued expansion of DMD-MuSCs is likely due to epigenetic drift where myogenic genes become repressed while genes of the fibroblast lineage become expressed. As broad genome epigenetic regulators, these factors may have interdependent control over each other expression in certain ways. For example, in the context of cancer cells, CBX3 was identified as a key player in cell proliferation and was reported to interact with the H3.3 histone variant at specific genes, including heat shock protein 70.[41] Studies have demonstrated that the recruitment of CBX3 and H3.3 at these genes is mutually dependent.[38] However, the precise nature of this interaction and its role in maintaining an open chromatin state at myogenic genes remains unclear, and beyond the scope of this study.

Our study has identified MEF2B as a key myogenic gene turned off during DMD-induced epigenetic drift. While MEF2 family of proteins has been widely studied in muscle, the MEF2B protein has largely been overlooked as a contributor to the myogenic fate. Among MEF2 family members, MEF2B presents a unique protein structure and does not bind the MEF2 consensus DNA motif because of the presence of its C-terminal domain.[48] While the role of Mef2b in murine myogenesis continues to be underappreciated,[49] our findings suggest that MEF2B is essential to maintaining the myogenic cell fate in humans. Indeed, we observed that exogenous expression of MEF2B in DMD-MuSCs reduced the loss of myogenic identity while depletion of MEF2B in MuSCs increased the rate at which the myogenic identity was lost. Interestingly, previous studies have hinted at a role for MEF2B in murine myogenesis. While *Mef2a*, *Mef2c*, and *Mef2d* are preferentially expressed in committed (MyoD-expressing) muscle progenitors, *Mef2b* is the predominant family member expressed in Pax7^{hi} MuSCs.[50] Lineage conversion experiments using mouse fibroblasts showed that *Pax7* (or *Pax3*) expression on its own was not sufficient to convert a fibroblast to the MuSC-like identity. However, a systematic analysis of MuSC-expressed transcription factors demonstrated that co-expression *Pax7* (or *Pax3*) with *Pitx1* and *Mef2b* resulted in the efficient conversion of fibroblasts to a MuSC-like lineage.[50] Interestingly, Pitx1 could be replaced by MyoD in these lineage conversion experiments, but Pax7/Pax3 and Mef2b remained essential to the reprogramming process.[50] Complementing these lineage conversion studies, our work shows that the loss of MEF2B leads to a loss of the myogenic identity with concomitant activation of fibrogenic gene expression, essentially a lineage conversion from MuSCs to the fibroblast lineage. Taken together, these results provide strong evidence that MEF2B is a key regulator of the early myogenic gene expression program and that the epigenetic regulators H3.3, CBX3, H2A.Z2, H3.3, and SMC3 play an essential role in ensuring the expression of this myogenic regulator to maintain lineage identity.

It is unclear whether the accelerated epigenetic drift observed in DMD-MuSCs is due to the loss of dystrophin itself, or due to downstream signaling initiated by the loss of dystrophin. In the absence of dystrophin in myofibers leads to mis-localization of the dystrophin-associated protein complex (DAPC) and the loss of nitric oxide synthase (NOS) signaling.[51,52] NOS signaling is necessary to regulate chromatin accessibility with the regulation of histone deacetylases (HDACs) in other different cell types.[53–55] In DMD myofibers, the absence of NOS signaling leads to aberrant activation of HDAC2 and global changes of histone acetylation across the genome.[56,57] The DAPC also regulates MuSC polarity and asymmetric division at the epigenetic level.[58,59] Moreover, in addition to the aberrant histone modification caused by the absence of dystrophin, it also leads to a deregulated ncRNA and genomic instability.[60–62] While we observe that DMD results in an epigenetic silencing of MEF2B expression

it remains unclear why the chromatin associated with this locus becomes transcriptionally repressive. However, it will be important to understand how this epigenetic drift occurs in DMD since many of the current therapy trials look to restore dystrophin expression, and have not examined restoration of downstream epigenetic pathways.

In that context, it is interesting to mention that some HDACs have been found to repress all MEF2 isoforms but MEF2B activity in muscle cells.[63] Since HDAC inhibitors improve DMD in mouse,[63] it would be interesting to test their impact on MEF2B in MuSCs.

An important finding of our studies is that DMD-MuSCs initially possess normal myogenic potential, but that this potential is lost over time due to epigenetic drift. While the properties of MuSCs have been extensively investigated, controversy in the field has persisted about the myogenic properties of MuSCs. Indeed, the study of DMD were hindered by two major hurdles: (1) investigation in mouse, using the mdx model, which poorly recapitulates DMD features and (2) investigation using human cells, that are no longer in their *in vivo* environment, with a risk of developing culture-driven artifacts. In its infancy, culture of human MuSCs was further limited by the presence of non-myogenic cells in the isolated cell population that were bulk cultured. Nevertheless, two types of cells were observed in those cultures, including myogenic cells, and cells that do not fuse and exhibit a fibroblastic phenotype, the number of which is increased in DMD samples as compared with normal muscle.[20,64,65] Clonal cultures confirmed the presence of non-fusing low creatine kinase activity cells along with myogenic cells, capable of fusion.[66,67] From the initial muscle samples, less cloneable MuSCs were obtained in DMD versus normal muscle[66,67] indicative of an enrichment of the diseased muscle by fibroblastic cells. Careful examination of the cell phenotype of unsorted cells, then culture of cells that were purified according to the CD56 expression showed that myogenic cells implement of normal myogenic process in DMD as compared with normal muscle, including proliferation, differentiation, and fusion.[19,68] In the present study, we also demonstrated that MuSCs that express CD56, and thus be considered as myogenic,[26] show unaltered myogenic properties. Similar results were observed in the large animal model GRMD dog.[69] Thus, as long as they are isolated as myogenic cells (expressing CD56), DMD-derived MuSCs have retained their full myogenic capacities.

Using purified CD56^{pos} MuSC cultures, we observed a progressive reduction in the proportion of myogenic cells with time. The loss of myogenicity has been repeatedly observed by other labs in cultures of human MuSCs isolated from normal (HC muscle, with very high variations between donors, and independently of their age and sex.[25,31,70] However, our results showed that the decrease in the proportion of myogenic CD56^{pos} cells was twice as fast in DMD cultures as compared with HC cultures. No difference was observed in the growth rate or apoptosis between CD56^{pos} and CD56^{neg} cell populations of both DMD and HC cell cultures, suggesting a transition of myogenic cells into fibroblastic cells with time. To validate this transition, we made clonal cultures of single CD56^{pos} cells that expressed Myf5 and found that these myogenic cells lose their myogenic nature and acquired the feature of fibroblasts by TCF7L2 expression while losing that of CD56. A few cells are double-positive, suggesting these cells are in transit between the two statuses. Such a transition was observed in normal MuSCs[25,70] where CD56^{neg} cells are capable of adipogenic differentiation while CD56^{pos} are not.[25,70] After the same period of time, DMD-MuSC-derived clones exhibit 3-fold more CD56^{neg} cells than HC-MuSC-derived cells, confirming that the transition occurs much faster in DMD cultures. This transition is associated with a general downregulation of the expression of several myogenic genes (*PAX7*, *ACTA1 MYF5*, and *MYOD*) with a concomitant increased expression of genes linked to a fibroblastic phenotype (*COL1A1*, *CTGF*, *LOX*, and *SPP1*). Such increase of gene associated with matrix deposition and matrix remodeling was previously reported in CD56^{pos} human MuSCs isolated from DMD muscle.[68] Whether this transition occurs in human *in vivo* is impossible to address. However, the presence of MuSCs expressing a canonical marker of fibrogenic cells (Pax7^{pos}; PDGFRa^{pos}) was reported in human DMD muscle.[18] Such a transition was previously shown *in vivo*, in the mdx mouse, where MuSCs harbor a fibrogenic plasticity. Using lineage tracing, a part of MuSCs lose their myogenic nature to acquire a fibrogenic identity, driven by a Wnt-TGFb axis.[16,18] In another muscle model of fibrosis, the number of myogenic progenitors expressing collagen I is also increased.[71] Thus, there is evidence that MuSCs, or a proportion of MuSCs, undergo epigenetic drift *in vivo* toward a fibroblast-like identity.

Despite our findings, the overall outcome of epigenetic drift on the number of MuSCs in dystrophic muscle is hard to determine. Indeed, several studies have described an increase in the number of MuSCs for both mouse mdx[72,73] and human DMD[74–78] muscles, while other studies have reported no differences.[79,80] In humans, the interpretation of the data is made even more difficult by the use of non-age-matched muscles.[74,77] In both mice and humans, the time of tissue sampling contributes to the difficulty in interpreting the data since at some specific ages there is no difference in the number of MuSCs between DMD and normal muscles.[72,78] Finally, in the double mdx/utn knockout (KO) mice, a model that better mimics the human disease pathology than mdx mice, the number of MuSCs is strongly reduced.[73] Interestingly, a study carefully measured the telomere length of freshly isolated MuSCs in normal and DMD context, both in mice and humans.[81] It showed that MuSCs from mdx and DMD muscles exhibit shorter telomere length, suggesting an impact on the cell behavior and function in DMD, in accordance with our data.

Limitations of the study

There are two main limitations of the present study. (1) A technical limitation. When DMD-MuSCs are isolated from the biopsy, the advancement of the disease is not known from patient to patient. Moreover, the number of passages required during the initial primary culture to expand the cells is not known. Although the cultures in the study are all analyzed from 100% CD56^{pos} cell populations, MuSCs may have experienced varying numbers of prior divisions. (2) A conceptual limitation. All the experiments described in this study were conducted with human cells, meaning that the conclusions raised are only based on *in vitro* data. Whether the phenotypic drift described here occurs similarly *in vivo* is, currently, impossible to address.

RESOURCE AVAILABILITY

Lead contact

Requests for further information and resources should be directed to and will be fulfilled by the lead contact, Bénédicte Chazaud (benedicte.chazaud@inserm.fr).

Materials availability

All unique/stable reagents generated in this study are available from the lead contact without restriction.

Data and code availability

- Raw data of transcriptome are deposited at GEO: GSE229968. Raw data of ATAC-seq are deposited at GEO: GSE232667. They are publicly available as of the date of publication.
- This paper does not report original code.
- Any additional information required to reanalyze the data reported in this paper is available from Bénédicte Chazaud (transcriptome) and Jeff Dilworth (ATAC-seq) upon request.

ACKNOWLEDGMENTS

We thank Pr Jamel Chelly for his support in initiating this work. This work was supported by FFCR (Fond Franco-Canadien pour la Recherche), Mitacs, Université Claude Bernard Lyon 1 to both B.C. and F.J.D. labs, AFM-Téléthon (Alliance MyoNeurALP), Inserm, CNRS (to B.C.), and CIHR (FDN143330 to F.J.D.). We thank the GENOMIC facility of Institut Cochin and the Cell Bank of Hopital Cochin.

AUTHOR CONTRIBUTIONS

Conceptualization: C.G., I.D., F.J.D., and B.C. Methodology and investigation: J.M., M.W.-G., H.B., M.M., A.H., P.N., S.G., and W.B. Analysis and validation: J.M., M.W.-G., F.J.D., B.C., S.G., and W.B. Resources: A.H., P.N., C.G., and I.D. Writing and visualization: J.M., M.W.-G., H.B., M.M., A.H., P.N., C.G., I.D., F.J.D., and B.C. Supervision and funding acquisition: F.J.D. and B.C.

DECLARATION OF INTERESTS

Authors declare no competing interests.

STAR★METHODS

Detailed methods are provided in the online version of this paper and include the following:

- KEY RESOURCES TABLE
- EXPERIMENTAL MODEL AND STUDY PARTICIPANT DETAILS
- METHOD DETAILS
  - Primary cultures of human MuSCs
  - Evaluation of CD56 expression by flow cytometry
  - Immuno-magnetic cell sorting
  - Proliferation assay
  - Myogenesis assay – differentiation
  - Myogenesis assay – fusion
  - TUNEL assay
  - Plasmid construction
  - Lentiviral production
  - MuSC lentiviral transduction and selection
  - Clonal cell culture
  - Quantitative RT-PCR
  - Transcriptomic analysis
  - Generation of a library for ATAC-seq
  - ATAC-seq data processing
  - CUT&Tag
  - Generation of the CUT&Tag library
  - Quantitative RT-PCR of CUT&Tag library
- QUANTIFICATION AND STATISTICAL ANALYSIS

SUPPLEMENTAL INFORMATION

Supplemental information can be found online at https://doi.org/10.1016/j.isci.2024.111350.

Received: May 30, 2023
Revised: June 21, 2024
Accepted: November 5, 2024
Published: November 8, 2024

REFERENCES

1. Wosczyna, M.N., and Rando, T.A. (2018). A Muscle Stem Cell Support Group: Coordinated Cellular Responses in Muscle Regeneration. Dev. Cell *46*, 135–143. https://doi.org/10.1016/j.devcel.2018.06.018.
2. Massenet, J., Gardner, E., Chazaud, B., and Dilworth, F.J. (2021). Epigenetic regulation of satellite cell fate during skeletal muscle regeneration. Skelet. Muscle *11*, 4. https://doi.org/10.1186/s13395-020-00259-w.
3. Asp, P., Blum, R., Vethantham, V., Parisi, F., Micsinai, M., Cheng, J., Bowman, C., Kluger, Y., and Dynlacht, B.D. (2011). Genome-wide remodeling of the epigenetic landscape during myogenic differentiation. Proc. Natl. Acad. Sci. USA *108*, E149–E158. https://doi.org/10.1073/pnas.1102223108.
4. Aziz, A., Liu, Q.C., and Dilworth, F.J. (2010). Regulating a master regulator: establishing tissue-specific gene expression in skeletal muscle. Epigenetics *5*, 691–695. https://doi.org/10.4161/epi.5.8.13045.
5. Segalés, J., Perdiguero, E., and Muñoz-Cánoves, P. (2015). Epigenetic control of adult skeletal muscle stem cell functions. FEBS J. *282*, 1571–1588. https://doi.org/10.1111/febs.13065.
6. Dalkilic, I., and Kunkel, L.M. (2003). Muscular dystrophies: genes to pathogenesis. Curr. Opin. Genet. Dev. *13*, 231–238. https://doi.org/10.1016/s0959-437x(03)00048-0.
7. Hoffman, E.P., Monaco, A.P., Feener, C.C., and Kunkel, L.M. (1987). Conservation of the Duchenne muscular dystrophy gene in mice and humans. Science *238*, 347–350. https://doi.org/10.1126/science.3659917.
8. Mendell, J.R., and Lloyd-Puryear, M. (2013). Report of MDA muscle disease symposium on newborn screening for Duchenne muscular dystrophy. Muscle Nerve *48*, 21–26. https://doi.org/10.1002/mus.23810.
9. Petrof, B.J., Shrager, J.B., Stedman, H.H., Kelly, A.M., and Sweeney, H.L. (1993). Dystrophin protects the sarcolemma from stresses developed during muscle contraction. Proc. Natl. Acad. Sci. USA *90*, 3710–3714. https://doi.org/10.1073/pnas.90.8.3710.
10. Williams, M.W., and Bloch, R.J. (1999). Differential distribution of dystrophin and beta-spectrin at the sarcolemma of fast twitch skeletal muscle fibers. J. Muscle Res. Cell Motil. *20*, 383–393. https://doi.org/10.1023/a:1005512217552.
11. Bareja, A., Holt, J.A., Luo, G., Chang, C., Lin, J., Hinken, A.C., Freudenberg, J.M., Kraus, W.E., Evans, W.J., and Billin, A.N. (2014). Human and mouse skeletal muscle stem cells: convergent and divergent mechanisms of myogenesis. PLoS One *9*, e90398. https://doi.org/10.1371/journal.pone.0090398.
12. Partridge, T.A. (2013). The mdx mouse model as a surrogate for Duchenne muscular dystrophy. FEBS J. *280*, 4177–4186. https://doi.org/10.1111/febs.12267.
13. Dumont, N.A., Wang, Y.X., and Rudnicki, M.A. (2015). Intrinsic and extrinsic mechanisms regulating satellite cell function. Development *142*, 1572–1581. https://doi.org/10.1242/dev.114223.
14. Yablonka-Reuveni, Z., and Anderson, J.E. (2006). Satellite cells from dystrophic (mdx) mice display accelerated differentiation in primary cultures and in isolated myofibers. Dev. Dyn. *235*, 203–212. https://doi.org/10.1002/dvdy.20602.

15. Boldrin, L., Zammit, P.S., and Morgan, J.E. (2015). Satellite cells from dystrophic muscle retain regenerative capacity. Stem Cell Res. *14*, 20–29. https://doi.org/10.1016/j.scr.2014.10.007.

16. Biressi, S., Miyabara, E.H., Gopinath, S.D., Carlig, P.M.M., and Rando, T.A. (2014). A Wnt-TGFβ2 axis induces a fibrogenic program in muscle stem cells from dystrophic mice. Sci. Transl. Med. *6*, 267ra176. https://doi.org/10.1126/scitranslmed.3008411.

17. Brack, A.S., Conboy, M.J., Roy, S., Lee, M., Kuo, C.J., Keller, C., and Rando, T.A. (2007). Increased Wnt signaling during aging alters muscle stem cell fate and increases fibrosis. Science *317*, 807–810. https://doi.org/10.1126/science.1144090.

18. Pessina, P., Kharraz, Y., Jardí, M., Fukada, S.I., Serrano, A.L., Perdiguero, E., and Muñoz-Cánoves, P. (2015). Fibrogenic Cell Plasticity Blunts Tissue Regeneration and Aggravates Muscular Dystrophy. Stem Cell Rep. *4*, 1046–1060. https://doi.org/10.1016/j.stemcr.2015.04.007.

19. Blau, H.M., Webster, C., Chiu, C.P., Guttman, S., and Chandler, F. (1983). Differentiation properties of pure populations of human dystrophic muscle cells. Exp. Cell Res. *144*, 495–503. https://doi.org/10.1016/0014-4827(83)90431-7.

20. Blau, H.M., Webster, C., and Pavlath, G.K. (1983). Defective myoblasts identified in Duchenne muscular dystrophy. Proc. Natl. Acad. Sci. USA *80*, 4856–4860. https://doi.org/10.1073/pnas.80.15.4856.

21. Franklin, G.I., Cavanagh, N.P., Hughes, B.P., Yasin, R., and Thompson, E.J. (1981). Creatine kinase isoenzymes in cultured human muscle cells. I. Comparison of Duchenne muscular dystrophy with other myopathic and neurogenic disease. Clin. Chim. Acta *115*, 179–189. https://doi.org/10.1016/0009-8981(81)90074-7.

22. Iannaccone, S.T., Nagy, B., and Samaha, F.J. (1987). Decreased creatine kinase activity in cultured Duchenne dystrophic muscle cells. J. Child Neurol. *2*, 17–21. https://doi.org/10.1177/088307388700200103.

23. Ionasescu, V., and Ionasescu, R. (1982). Increased collagen synthesis by Duchenne myogenic clones. J. Neurol. Sci. *54*, 79–87.

24. Jasmin, G., Tautu, C., Vanasse, M., Brochu, P., and Simoneau, R. (1984). Impaired muscle differentiation in explant cultures of Duchenne muscular dystrophy. Lab. Invest. *50*, 197–207.

25. Agley, C.C., Rowlerson, A.M., Velloso, C.P., Lazarus, N.R., and Harridge, S.D.R. (2013). Human skeletal muscle fibroblasts, but not myogenic cells, readily undergo adipogenic differentiation. J. Cell Sci. *126*, 5610–5625.

26. Illa, I., Leon-Monzon, M., and Dalakas, M.C. (1992). Regenerating and denervated human muscle fibers and satellite cells express neural cell adhesion molecule recognized by monoclonal antibodies to natural killer cells. Ann. Neurol. *31*, 46–52. http://www.ncbi.nlm.nih.gov/entrez/query.fcgi?cmd=Retrieve&db=PubMed&dopt=Citation&list_uids=1371910.

27. Mackey, A.L., Kjaer, M., Charifi, N., Henriksson, J., Bojsen-Moller, J., Holm, L., and Kadi, F. (2009). Assessment of satellite cell number and activity status in human skeletal muscle biopsies. Muscle Nerve *40*, 455–465.

28. Stewart, J.D., Masi, T.L., Cumming, A.E., Molnar, G.M., Wentworth, B.M., Sampath, K., McPherson, J.M., and Yaeger, P.C. (2003). Characterization of proliferating human skeletal muscle-derived cells *in vitro*: Differential modulation of myoblast markers by TGF-beta2. J. Cell. Physiol. *196*, 70–78.

29. Uezumi, A., Nakatani, M., Ikemoto-Uezumi, M., Yamamoto, N., Morita, M., Yamaguchi, A., Yamada, H., Kasai, T., Masuda, S., Narita, A., et al. (2016). Cell-Surface Protein Profiling Identifies Distinctive Markers of Progenitor Cells in Human Skeletal Muscle. Stem Cell Rep. *7*, 263–278. https://doi.org/10.1016/j.stemcr.2016.07.004.

30. Xu, X., Wilschut, K.J., Kouklis, G., Tian, H., Hesse, R., Garland, C., Sbitany, H., Hansen, S., Seth, R., Knott, P.D., et al. (2015). Human Satellite Cell Transplantation and Regeneration from Diverse Skeletal Muscles. Stem Cell Rep. *5*, 419–434. https://doi.org/10.1016/j.stemcr.2015.07.016.

31. Alsharidah, M., Lazarus, N.R., George, T.E., Agley, C.C., Velloso, C.P., and Harridge, S.D.R. (2013). Primary human muscle precursor cells obtained from young and old donors produce similar proliferative, differentiation and senescent profiles in culture. Aging Cell *12*, 333–344.

32. Kim, S., Jung, P.Y., Lee, J.S., Hwang, S., Sohn, J.H., Yoon, Y., Bae, K.S., and Eom, Y.W. (2021). Cultured human skeletal muscle satellite cells exhibit characteristics of mesenchymal stem cells and play anti-inflammatory roles through prostaglandin E2 and hepatocyte growth factors. Cell Biol. Int. *45*, 2443–2451. https://doi.org/10.1002/cbin.11688.

33. Farup, J., Just, J., de Paoli, F., Lin, L., Jensen, J.B., Billeskov, T., Roman, I.S., Cömert, C., Møller, A.B., Madaro, L., et al. (2021). Human skeletal muscle CD90(+) fibro-adipogenic progenitors are associated with muscle degeneration in type 2 diabetic patients. Cell Metab. *33*, 2201–2214.e11. https://doi.org/10.1016/j.cmet.2021.10.001.

34. Mackey, A.L., Magnan, M., Chazaud, B., and Kjaer, M. (2017). Human skeletal muscle fibroblasts stimulate *in vitro* myogenesis and *in vivo* muscle regeneration. J. Physiol. *595*, 5115–5127. https://doi.org/10.1113/jp273997.

35. Massenet, J., Gitiaux, C., Magnan, M., Cuvellier, S., Hubas, A., Nusbaum, P., Dilworth, F.J., Desguerre, I., and Chazaud, B. (2020). Derivation and Characterization of Immortalized Human Muscle Satellite Cell Clones from Muscular Dystrophy Patients and Healthy Individuals. Cells *9*, 1780. https://doi.org/10.3390/cells9081780.

36. Dall'Agnese, A., Caputo, L., Nicoletti, C., di Iulio, J., Schmitt, A., Gatto, S., Diao, Y., Ye, Z., Forcato, M., Perera, R., et al. (2019). Transcription Factor-Directed Re-wiring of Chromatin Architecture for Somatic Cell Nuclear Reprogramming toward trans-Differentiation. Mol. Cell *76*, 453–472.e8. https://doi.org/10.1016/j.molcel.2019.07.036.

37. Hansen, A.S., Cattoglio, C., Darzacq, X., and Tjian, R. (2018). Recent evidence that TADs and chromatin loops are dynamic structures. Nucleus *9*, 20–32. https://doi.org/10.1080/19491034.2017.1389365.

38. Kim, H., Heo, K., Choi, J., Kim, K., and An, W. (2011). Histone variant H3.3 stimulates HSP70 transcription through cooperation with HP1γ. Nucleic Acids Res. *39*, 8329–8341. https://doi.org/10.1093/nar/gkr529.

39. Schoelz, J.M., and Riddle, N.C. (2022). Functions of HP1 proteins in transcriptional regulation. Epigenet. Chromatin *15*, 14. https://doi.org/10.1186/s13072-022-00453-8.

40. Yahi, H., Fritsch, L., Philipot, O., Guasconi, V., Souidi, M., Robin, P., Polesskaya, A., Losson, R., Harel-Bellan, A., and Ait-Si-Ali, S. (2008). Differential cooperation between heterochromatin protein HP1 isoforms and MyoD in myoblasts. J. Biol. Chem. *283*, 23692–23700. https://doi.org/10.1074/jbc.M802647200.

41. Zhong, X., Kan, A., Zhang, W., Zhou, J., Zhang, H., Chen, J., and Tang, S. (2019). CBX3/HP1γ promotes tumor proliferation and predicts poor survival in hepatocellular carcinoma. Aging (Albany NY) *11*, 5483–5497. https://doi.org/10.18632/aging.102132.

42. Jin, C., Zang, C., Wei, G., Cui, K., Peng, W., Zhao, K., and Felsenfeld, G. (2009). H3.3/H2A.Z double variant-containing nucleosomes mark 'nucleosome-free regions' of active promoters and other regulatory regions. Nat. Genet. *41*, 941–945. https://doi.org/10.1038/ng.409.

43. Santisteban, M.S., Kalashnikova, T., and Smith, M.M. (2000). Histone H2A.Z regulats transcription and is partially redundant with nucleosome remodeling complexes. Cell *103*, 411–422. https://doi.org/10.1016/s0092-8674(00)00133-1.

44. Vardabasso, C., Gaspar-Maia, A., Hasson, D., Pünzeler, S., Valle-Garcia, D., Straub, T., Keilhauer, E.C., Strub, T., Dong, J., Panda, T., et al. (2015). Histone Variant H2A.Z.2 Mediates Proliferation and Drug Sensitivity of Malignant Melanoma. Mol. Cell *59*, 75–88. https://doi.org/10.1016/j.molcel.2015.05.009.

45. Harada, A., Okada, S., Konno, D., Odawara, J., Yoshimi, T., Yoshimura, S., Kumamaru, H., Saiwai, H., Tsubota, T., Kurumizaka, H., et al. (2012). Chd2 interacts with H3.3 to determine myogenic cell fate. EMBO J. *31*, 2994–3007. https://doi.org/10.1038/emboj.2012.136.

46. Ng, R.K., and Gurdon, J.B. (2008). Epigenetic memory of an active gene state depends on histone H3.3 incorporation into chromatin in the

absence of transcription. Nat. Cell Biol. *10*, 102–109. https://doi.org/10.1038/ncb1674.

47. Esteves de Lima, J., Bou Akar, R., Machado, L., Li, Y., Drayton-Libotte, B., Dilworth, F.J., and Relaix, F. (2021). HIRA stabilizes skeletal muscle lineage identity. Nat. Commun. *12*, 3450. https://doi.org/10.1038/s41467-021-23775-9.
48. Molkentin, J.D., Firulli, A.B., Black, B.L., Martin, J.F., Hustad, C.M., Copeland, N., Jenkins, N., Lyons, G., and Olson, E.N. (1996). MEF2B is a potent transactivator expressed in early myogenic lineages. Mol. Cell Biol. *16*, 3814–3824. https://doi.org/10.1128/mcb.16.7.3814.
49. Morisaki, T., Sermsuvitayawong, K., Byun, S.H., Matsuda, Y., Hidaka, K., Morisaki, H., and Mukai, T. (1997). Mouse Mef2b gene: unique member of MEF2 gene family. J. Biochem. *122*, 939–946. https://doi.org/10.1093/oxfordjournals.jbchem.a021855.
50. Ito, N., Kii, I., Shimizu, N., Tanaka, H., and Takeda, S. (2017). Direct reprogramming of fibroblasts into skeletal muscle progenitor cells by transcription factors enriched in undifferentiated subpopulation of satellite cells. Sci. Rep. *7*, 8097. https://doi.org/10.1038/s41598-017-08232-2.
51. Brenman, J.E., Chao, D.S., Xia, H., Aldape, K., and Bredt, D.S. (1995). Nitric oxide synthase complexed with dystrophin and absent from skeletal muscle sarcolemma in Duchenne muscular dystrophy. Cell *82*, 743–752. https://doi.org/10.1016/0092-8674(95)90471-9.
52. Lai, Y., Thomas, G.D., Yue, Y., Yang, H.T., Li, D., Long, C., Judge, L., Bostick, B., Chamberlain, J.S., Terjung, R.L., and Duan, D. (2009). Dystrophins carrying spectrin-like repeats 16 and 17 anchor nNOS to the sarcolemma and enhance exercise performance in a mouse model of muscular dystrophy. J. Clin. Invest. *119*, 624–635. https://doi.org/10.1172/jci36612.
53. Mengel, A., Ageeva, A., Georgii, E., Bernhardt, J., Wu, K., Durner, J., and Lindermayr, C. (2017). Nitric Oxide Modulates Histone Acetylation at Stress Genes by Inhibition of Histone Deacetylases. Plant Physiol. *173*, 1434–1452. https://doi.org/10.1104/pp.16.01734.
54. Nott, A., Watson, P.M., Robinson, J.D., Crepaldi, L., and Riccio, A. (2008). S-Nitrosylation of histone deacetylase 2 induces chromatin remodelling in neurons. Nature *455*, 411–415. https://doi.org/10.1038/nature07238.
55. Vasudevan, D., Bovee, R.C., and Thomas, D.D. (2016). Nitric oxide, the new architect of epigenetic landscapes. Nitric Oxide *59*, 54–62. https://doi.org/10.1016/j.niox.2016.08.002.
56. Colussi, C., Gurtner, A., Rosati, J., Illi, B., Ragone, G., Piaggio, G., Moggio, M., Lamperti, C., D'Angelo, G., Clementi, E., et al. (2009). Nitric oxide deficiency determines global chromatin changes in Duchenne muscular dystrophy. FASEB J. *23*, 2131–2141. https://doi.org/10.1096/fj.08-115618.
57. Illi, B., Dello Russo, C., Colussi, C., Rosati, J., Pallaoro, M., Spallotta, F., Rotili, D., Valente, S., Ragone, G., Martelli, F., et al. (2008). Nitric oxide modulates chromatin folding in human endothelial cells via protein phosphatase 2A activation and class II histone deacetylases nuclear shuttling. Circ. Res. *102*, 51–58. https://doi.org/10.1161/circresaha.107.157305.
58. Chang, N.C., Sincennes, M.C., Chevalier, F.P., Brun, C.E., Lacaria, M., Segalés, J., Muñoz-Cánoves, P., Ming, H., and Rudnicki, M.A. (2018). The Dystrophin Glycoprotein Complex Regulates the Epigenetic Activation of Muscle Stem Cell Commitment. Cell Stem Cell *22*, 755–768.e6. https://doi.org/10.1016/j.stem.2018.03.022.
59. Dumont, N.A., Wang, Y.X., von Maltzahn, J., Pasut, A., Bentzinger, C.F., Brun, C.E., and Rudnicki, M.A. (2015). Dystrophin expression in muscle stem cells regulates their polarity and asymmetric division. Nat. Med. *21*, 1455–1463. https://doi.org/10.1038/nm.3990.
60. Cacchiarelli, D., Martone, J., Girardi, E., Cesana, M., Incitti, T., Morlando, M., Nicoletti, C., Santini, T., Sthandier, O., Barberi, L., et al. (2010). MicroRNAs involved in molecular circuitries relevant for the Duchenne muscular dystrophy pathogenesis are controlled by the dystrophin/nNOS pathway. Cell Metab. *12*, 341–351. https://doi.org/10.1016/j.cmet.2010.07.008.
61. Iyer, S.R., Shah, S.B., Ward, C.W., Stains, J.P., Spangenburg, E.E., Folker, E.S., and Lovering, R.M. (2019). Differential YAP nuclear signaling in healthy and dystrophic skeletal muscle. Am. J. Physiol. Cell Physiol. *317*, C48–C57. https://doi.org/10.1152/ajpcell.00432.2018.
62. Schmidt, W.M., Uddin, M.H., Dysek, S., Moser-Thier, K., Pirker, C., Höger, H., Ambros, I.M., Ambros, P.F., Berger, W., and Bittner, R.E. (2011). DNA damage, somatic aneuploidy, and malignant sarcoma susceptibility in muscular dystrophies. PLoS Genet. *7*, e1002042. https://doi.org/10.1371/journal.pgen.1002042.
63. Mozzetta, C., Sartorelli, V., Steinkuhler, C., and Puri, P.L. (2024). HDAC inhibitors as pharmacological treatment for Duchenne muscular dystrophy: a discovery journey from bench to patients. Trends Mol. Med. *30*, 278–294. https://doi.org/10.1016/j.molmed.2024.01.007.
64. Delaporte, C., Dehaupas, M., and Fardeau, M. (1984). Comparison between the growth pattern of cell cultures from normal and Duchenne dystrophy muscle. J. Neurol. Sci. *64*, 149–160.
65. Yasin, R., Van Beers, G., Riddle, P.N., Brown, D., Widdowson, G., and Thompson, E.J. (1979). An abnormality of cell behaviour in human dystrophic muscle cultures: a time-lapse study. J. Cell Sci. *38*, 201–210.
66. Meola, G., Velicogna, M., Brigato, C., Pizzul, S., Rotondo, G., and Scarlato, G. (1991). Growth and differentiation of myogenic clones from adult human muscle cell cultures. Eur. J. Basic Appl. Histochem. *35*, 219–231.
67. Webster, C., and Blau, H.M. (1990). Accelerated age-related decline in replicative life-span of Duchenne muscular dystrophy myoblasts: implications for cell and gene therapy. Somat. Cell Mol. Genet. *16*, 557–565.
68. Zanotti, S., Saredi, S., Ruggieri, A., Fabbri, M., Blasevich, F., Romaggi, S., Morandi, L., and Mora, M. (2007). Altered extracellular matrix transcript expression and protein modulation in primary Duchenne muscular dystrophy myotubes. Matrix Biol. *26*, 615–624.
69. Berg, Z., Beffa, L.R., Cook, D.P., and Cornelison, D.D.W. (2011). Muscle satellite cells from GRMD dystrophic dogs are not phenotypically distinguishable from wild type satellite cells in ex vivo culture. Neuromuscul. Disord. *21*, 282–290.
70. Francis, T.G., Jaka, O., Ellison-Hughes, G.M., Lazarus, N.R., and Harridge, S.D. (2022). Human primary skeletal muscle-derived myoblasts and fibroblasts reveal different senescent phenotypes. JCSM Rapid Commun. *5*, 226–238. https://doi.org/10.1002/rco2.67.
71. Chapman, M.A., Mukund, K., Subramaniam, S., Brenner, D., and Lieber, R.L. (2017). Three distinct cell populations express extracellular matrix proteins and increase in number during skeletal muscle fibrosis. Am. J. Physiol. Cell Physiol. *312*, C131–C143. https://doi.org/10.1152/ajpcell.00226.2016.
72. Jiang, C., Wen, Y., Kuroda, K., Hannon, K., Rudnicki, M.A., and Kuang, S. (2014). Notch signaling deficiency underlies age-dependent depletion of satellite cells in muscular dystrophy. Dis. Model. Mech. *7*, 997–1004. https://doi.org/10.1242/dmm.015917.
73. Lu, A., Poddar, M., Tang, Y., Proto, J.D., Sohn, J., Mu, X., Oyster, N., Wang, B., and Huard, J. (2014). Rapid depletion of muscle progenitor cells in dystrophic mdx/utrophin-/- mice. Hum. Mol. Genet. *23*, 4786–4800. https://doi.org/10.1093/hmg/ddu194.
74. Bankolé, L.C., Feasson, L., Ponsot, E., and Kadi, F. (2013). Fibre type-specific satellite cell content in two models of muscle disease. Histopathology *63*, 826–832. https://doi.org/10.1111/his.12231.
75. Ishimoto, S., Goto, I., Ohta, M., and Kuroiwa, Y. (1983). A quantitative study of the muscle satellite cells in various neuromuscular disorders. J. Neurol. Sci. *62*, 303–314. https://doi.org/10.1016/0022-510x(83)90207-1.
76. Kottlors, M., and Kirschner, J. (2010). Elevated satellite cell number in Duchenne muscular dystrophy. Cell Tissue Res. *340*, 541–548. https://doi.org/10.1007/s00441-010-0976-6.
77. Maier, F., and Bornemann, A. (1999). Comparison of the muscle fiber diameter and satellite cell frequency in human muscle biopsies. Muscle Nerve *22*, 578–583. https://doi.org/10.1002/(sici)1097-4598(199905)22:5<578::aid-mus5>3.0.co;2-t.

78. Wakayama, Y., Schotland, D.L., Bonilla, E., and Orecchio, E. (1979). Quantitative ultrastructural study of muscle satellite cells in Duchenne dystrophy. Neurology *29*, 401–407. https://doi.org/10.1212/wnl.29.3.401.

79. Hussein, M.R.A., Abu-Dief, E.E., Kamel, N.F., and Mostafa, M.G. (2010). Steroid therapy is associated with decreased numbers of dendritic cells and fibroblasts, and increased numbers of satellite cells, in the dystrophic skeletal muscle. J. Clin. Pathol. *63*, 805–813. https://doi.org/10.1136/jcp.2010.078204.

80. Reimann, J., Irintchev, A., and Wernig, A. (2000). Regenerative capacity and the number of satellite cells in soleus muscles of normal and mdx mice. Neuromuscul. Disord. *10*, 276–282. https://doi.org/10.1016/s0960-8966(99)00118-2.

81. Tichy, E.D., Sidibe, D.K., Tierney, M.T., Stec, M.J., Sharifi-Sanjani, M., Hosalkar, H., Mubarak, S., Johnson, F.B., Sacco, A., and Mourkioti, F. (2017). Single Stem Cell Imaging and Analysis Reveals Telomere Length Differences in Diseased Human and Mouse Skeletal Muscles. Stem Cell Rep. *9*, 1328–1341. https://doi.org/10.1016/j.stemcr.2017.08.003.

82. Hildyard, J.C.W., and Wells, D.J. (2014). Identification and validation of quantitative PCR reference genes suitable for normalizing expression in normal and dystrophic cell culture models of myogenesis. PLoS Curr. *6*, ecurrents.md.faafdde4bea8df4aa7d06cd5553119a5553116. https://doi.org/10.1371/currents.md.faafdde4bea8df4aa7d06cd5553119a6.

83. Corces, M.R., Trevino, A.E., Hamilton, E.G., Greenside, P.G., Sinnott-Armstrong, N.A., Vesuna, S., Satpathy, A.T., Rubin, A.J., Montine, K.S., Wu, B., et al. (2017). An improved ATAC-seq protocol reduces background and enables interrogation of frozen tissues. Nat. Methods *14*, 959–962. https://doi.org/10.1038/nmeth.4396.

84. Li, Y., Nakka, K., Olender, T., Gingras-Gelinas, P., Wong, M.M.K., Robinson, D.C.L., Bandukwala, H., Palii, C.G., Neyret, O., Brand, M., et al. (2021). Chromatin and transcription factor profiling in rare stem cell populations using CUT&Tag. STAR Protoc. *2*, 100751. https://doi.org/10.1016/j.xpro.2021.100751.

85. Buenrostro, J.D., Wu, B., Litzenburger, U.M., Ruff, D., Gonzales, M.L., Snyder, M.P., Chang, H.Y., and Greenleaf, W.J. (2015). Single-cell chromatin accessibility reveals principles of regulatory variation. Nature *523*, 486–490. https://doi.org/10.1038/nature14590.

STAR★METHODS

KEY RESOURCES TABLE

REAGENT or RESOURCE	SOURCE	IDENTIFIER
Antibodies		
anti-CD56 mouse antibodies	Coulter Clone	#PN4235479-G
anti-desmin rabbit antibodies	Abcam	#ab32362 RRID:AB_731901
anti-HA antibodies	Roche	11583816001 RRID:AB_514505
anti-myogenin mouse antibodies	BD Biosciences	#556358 RRID:AB_396383
anti-Pax7 rabbit antibodies	Abcam	#ab92317 RRID:AB_10561454
anti-TCF7L2 rabbit antibodies	Cell Signaling Technology	#C48H11 RRID:AB_2199816
APC-conjugated anti-CD56 antibodies	BD Pharmingen	#555518 RRID:AB_398601
CD56 primary antibody	Miltenyi	#130-050-401 RRID:AB_3076236
Cy3-coupled anti-mouse IgGs	Jackson ImmunoResearch	#715-165-150 RRID:AB_2340813
Cy5-coupled anti-rabbit IgGs	Jackson ImmunoResearch	#711-165-152 RRID:AB_2307443
isotype control	BD Pharmingen	#555751 RRID:AB_398613
mouse anti-IgGs antibodies	Abcam	#ab6708 RRID:AB_956005
rabbit anti-H3K4me3 antibodies	Sigma	#04-745 RRID:AB_1163444
Biological samples		
MuSCs from patients	Cochin Hospital Cell Bank, Paris	agreement n°DC-2009-944
Chemicals, peptides, and recombinant proteins		
concanavalin A coated magnetic beads	Bangs Laboratories	#BP531
Fetal Bovine Serum	Abcys	#S1810-500
Fluoromount	Sigma	#F4680
Hoechst	Sigma	#B2261
human insulin	Sigma	#I2643
M-MuLV Reverse Transcriptase	NEB	#M0253L
NEBNext HiFi 2X PCR master mix	NEB	#M0544
penicillin streptomycin	Gibco	#15140
Phusion High-Fidelity DNA Polymerase	NEB	#M0530S
polybrene	Sigma	#107689
puromycin	Sigma	#P8833
Skeletal Muscle Cell Growth Medium	Promocell	#C23260
skeletal muscle supplemental mix	Promocell	#C39365
Superscript II Reverse Transcriptase	ThermoFisher	#18064022
SureSelectQXT Library Prep for WGS	Agilent	#9684
T4 DNA ligase	NEB	#M0202L
Critical commercial assays		
Click-iT EdU Alexa Fluor 488 Imaging Kit	ThermoFisher	#C10337
Click-iT™ Plus TUNEL Assay	ThermoFisher	#C10617
CloneEZ PCR Cloning Kit	GenScript	#L00339
NucleoSpin RNA Plus XS kit	Macherey-Nagel	#740990.50
LightCycler 480 SYBR Green I Master Kit	LifeSciences	#04707518001
Affymetrix GeneChip Human 8X60K chip	Affymetrix	8X60K
DNA Clean & Concentrator-TM-5 kit	Zymo	#D4003
GeneJET PCR Purification kit	Thermo Scientific	#K0701
Deposited data		
Tanscriptome data	This study	GSE229968

(*Continued on next page*)

Continued		
REAGENT or RESOURCE	SOURCE	IDENTIFIER
The ATACseq data	This study	GSE232667
Experimental models: Cell lines		
HEK293T cells		
Oligonucleotides		
CCGGGCCTCTTCAGAGAAGACCCAACTCGAG TTGGGTCTTCTCTGAAGAGGCTTTTT	Sigma	#SHCLNG
CCGGGCCAACCGCCTCTTCCAGTATCTCGAG ATACTGGAAGAGGCGGTTGGCTTTTT	Sigma	#SHCLNG
CCGGGGACTAAACACCTCCAGAAGCCTCGAG GCTTCTGGAGGTGTTTAGTCCTTTTTG	Sigma	#SHCLNG
CCGGCCCAGTCAGCATCAAGTCTGACTCGAG TCAGACTTGATGCTGACTGGGTTTTTG	Sigma	#SHCLNG
See Table S3 for RT-qPCR primers		
Recombinant DNA		
pLenti-EF1a-SetD2-HA plasmid	ABMgood	#435220610695
pLenti-GIII-EF1a-HA plasmid(	ABMgood	#2832406
pLKO.1 plasmid backbone	ABMgood	#10878
pLenti-GIII-EF1a empty	ABMgood	#LV588
MD2.G plasmid	Addgene	#12259
psPax2 plasmid	Addgene	#12260
Software and algorithms		
DAVID gene ontology software	https://david.ncifcrf.gov/	
Cutadapt 2.6.	https://cutadapt.readthedocs.io/en/v2.6/installation.html	
Bowtie 2 v2.3.4.1.	https://bowtie-bio.sourceforge.net/bowtie2/	
Samtools v1.10	https://github.com/samtools/samtools/releases/	
MACS2 2.1.2	https://pypi.org/project/MACS2/	
ChIPseeker 3.1.1.	https://guangchuangyu.github.io/2014/04/chipseeker-for-chip-peak-annotation/	.

EXPERIMENTAL MODEL AND STUDY PARTICIPANT DETAILS

Biopsies were obtained from *deltoideus medialis* of 21 genetically characterized DMD patients. Fourteen patients (males) undergoing orthopedic surgery (intercostal muscle) or for which the deltoid biopsy showed no signs of neuromuscular diseases and for whom the diagnosis workup was normal were used as age-matched controls (2-15 year-old). Written informed consent was obtained from all patients (or legal representatives) for the use of their biopsy for research purposes. The whole procedure was handled by the Cochin Hospital Cell Bank, Paris. Cells were recovered from the hospital cell bank (protocol registered at the Ministère de la Recherche and Cochin Hospital Cell Bank, Paris, agreement n°DC-2009-944).

METHOD DETAILS

Primary cultures of human MuSCs

From the muscle biopsy to the delivery by the cell bank, muscle cells were expanded for about 7-10 days before magnetic cell sorting based on CD56 expression was performed (Figure S1A). Purity of the cells was evaluated after flow cytometry evaluation of CD56 expression (see below) and by immunofluorescence (IF) after 6h of culture on glass coverslips. After fixation (paraformaldehyde [PFA] 4%) and permeabilization (triton X-100 0.5%), cells were incubated with anti-CD56 mouse antibodies (1:10, Coulter Clone #PN4235479-G) and anti-Pax7 rabbit antibodies (1:200, Abcam #ab92317) overnight at 4°C, that were revealed by Cy3-coupled anti-mouse IgGs (1:200, Jackson ImmunoResearch #715-165-150) and Cy5-coupled anti-rabbit IgGs (1:200, Jackson ImmunoResearch #711-165-152) for 45 min at 37°C. Nuclei were labeled with Hoechst (Sigma #B2261) and mounting was done in Fluoromount (Sigma #F4680). Primary cells were cultured in growth medium, which includes Skeletal Muscle Cell Growth Medium

(Promocell #C23260) containing skeletal muscle supplemental mix (Promocell #C39365), 10% of Fetal Bovine Serum (FBS) (Abcys #S1810-500), 100 U/ml penicillin and 100 μg/ml streptomycin (Gibco #15140).

Evaluation of CD56 expression by flow cytometry

Trypsinized or MACS sorted cells were incubated at 4°C for 20 min with APC-conjugated anti-CD56 antibodies (1:40, BD Pharmingen #555518) or isotype control (1:40, BD Pharmingen #555751) and further analyzed using a FACSCanto II flow cytometer (BD Biosciences).

Immuno-magnetic cell sorting

Cells were trypsinized, centrifuged and resuspended in 170 μl of magnetic-activated cell sorting (MACS) buffer (Phosphate-Buffered Saline solution (PBS) containing 5% Bovine Serum Albumin (BSA, Sigma #A9647), 1 mol/l of Ethylenediaminetetraacetic Acid Disodium (EDTA, Sigma #ED2SS). Thirty μl of superparamagnetic microbeads conjugated to a CD56 primary antibody (Miltenyi #130-050-401) was mixed with the cell suspension and incubated for 30 min at 4°C. After a wash with MACS buffer, the cell suspension was passed through a 30 μm filter (Miltenyi #130-041-407) and dripped into a LC column (Miltenyi #130-042-202) held in a MiniMACS magnetic separation unit (Miltenyi). Eluted cells were recovered as $CD56^{neg}$ cells. Column was then removed from the magnetic separation unit, and flushed with MACS buffer to recover $CD56^{pos}$ cells.

Proliferation assay

$CD56^{pos}$ cells were seeded at 3,000 cells per cm^2 in 4 well Permanox Nunc Lab-Tek chambers (ThermoFisher #177437) and cultured in growth medium. Two days later, EdU (Click-iT EdU Alexa Fluor 488 Imaging Kit, ThermoFisher #C10337) was added at 1 μg/ml and cells were further incubated for 8 h and then processed following the manufacturer's instructions. Nuclei were labeled with Hoechst and mounting was done in Fluoromount. The percentage of proliferating cells was calculated as the number of Alexa fluor-488 positive nuclei over the total number of nuclei.

Myogenesis assay – differentiation

Freshly $CD56^{pos}$ sorted cells were seeded at 1,000 cells per cm^2 in 4 well Permanox Nunc Lab-Tek chambers in growth medium. Six h later, medium was replaced by differentiation medium (Skeletal Muscle Basal Medium containing 10 μg/ml human insulin [Sigma #I2643]) and cells were cultured for 5 days. Long term cultured transduced cells were seeded at 10,000 cells per cm^2 in 8 well Permanox Nunc Lab-Tek chambers (ThermoFisher #177402) and grown for 5 days in growth medium. Then, differentiation medium was added and cells were further incubated 7 days. IF was performed as described above using anti-myogenin mouse antibodies (1:50, BD Biosciences #556358) and anti-desmin rabbit antibodies (1:200, Abcam #ab32362) revealed by Cy3-coupled anti-mouse IgGs and Cy5-coupled anti-rabbit IgGs. The percentage of differentiated cells was calculated as the number of cells positive for myogenin nuclei over the total number of cells.

Myogenesis assay – fusion

Freshly $CD56^{pos}$ cells were plated at 500 cells per cm^2 in 175 cm^2 Nunc Flask (ThermoFisher #156502) in growth medium. Six h later, medium was replaced by differentiation medium and cells were cultured for 5 days. Then, these differentiated cells were trypsinized and seeded at 50,000 cells per cm^2 in 8 well permanox Nunc Lab-Tek chambers in growth medium. Six h later, growth medium was replaced by differentiation medium and cells were cultured for 3 days. Long term cultured transduced cells were seeded at 10,000 cells per cm^2 in 8 well permanox Nunc Lab-Tek chambers. After 5 days of culture in growth medium, differentiation medium was added and cells were cultured 7 days more. IF was performed as described above using anti-desmin rabbit antibodies revealed by Cy5-coupled anti-rabbit IgGs. The fusion index was calculated as the number of nuclei in cells presenting two or more nuclei over the total number of nuclei.

TUNEL assay

Cells were seeded at 3,000 cells per cm^2 in 12-well plates containing glass coverslips and were incubated for 24 h. After PFA fixation and Triton permeabilization, cells were stained for DNA strand break using Click-iT™ Plus TUNEL Assay (ThermoFisher #C10617) following manufacturer's protocol before mounting in Fluoromount.

Plasmid construction

The pLenti-GIII-EF1a-linker-Flag-Hemagglutinin(HA) plasmid was built by insertion of a linker sequence containing cutting sites in the pLenti-EF1a-SetD2-HA plasmid (ABMgood #435220610695), digested at cutting sites of EcoRV, with CloneEZ PCR Cloning Kit (GenScript #L00339). The pLenti-GIII-EF1a-CBX3-Flag-HA, pLenti-GIII-EF1a-H2AZ2-Flag-HA, pLenti-GIII-EF1a-H3F3B-Flag-HA and pLenti-GIII-EF1a-SMC3-Flag-HA plasmids were built by insertion of a PCR amplified CBX3, H2AZ2, H3F3B or SMC3 gene cDNA in the pLenti-EF1a-linker-Flag-HA plasmid, digested at cutting sites BamHI and KpnI for H2AZ2, NheI and XbaI for H3F3B, of EcoRV, using the CloneEZ PCR Cloning Kit. The PCR amplification of CBX3, H2AZ2, H3F3B or SMC3 was performed with Phusion High-Fidelity DNA Polymerase (NEB #M0530S) on human MuSC cDNA. The cDNAs were built by reverse transcription of proliferating MuSC mRNAs using M-MuLV Reverse Transcriptase (NEB #M0253L). mRNAs were extracted using NucleoSpin RNA Plus XS kit

(Macherey-Nagel #740990.50). MEF2B was cloned in pLenti-GIII-EF1a-HA plasmid by abmgood using NheI and BamHI cutting sites (ABMgood, #2832406). The pLV-Myf5Promoter-GFP plasmid was built by insertion of two sequences in a pLKO.1 plasmid backbone (Addgene #10878). The Myf5-promoter sequence was added at NdeI and KpeI cutting sites and the CRE-GFP sequence was added at SpeI and XhoI restriction sites using a T4 DNA ligase (NEB #M0202L). Linker sequence and primers used for PCR amplification are listed in Table S3. The MEF2B shRNA sequences inserted in a pLKO-1 puro plasmid are listed in Table S4 (Sigma, #SHCLNG).

Lentiviral production

Lentiviral production was carried out by CaCl2 transfection of HEK293T cells ($1x10^6$ cells) using 19.9 μg of constructed lentiviral vector or a pLenti-GIII-EF1a empty (ABMgood #LV588), 5.93 μg of MD2.G plasmid (Addgene #12259) and 14.88 μg of psPax2 plasmid (Addgene #12260) during 15 h. Supernatant containing lentivirus was collected 24 and 48 h after the end of transfection, filtered and concentrated using sucrose buffer and ultracentrifugation at 120,000 g for 2 h at 4°C. Lentiviral titration was estimated by transfection of healthy MuSCs with concentrated lentivirus in growth medium supplemented by 6 μg/ml of polybrene (Sigma #107689). One day after transfection, cells were selected in growth medium supplemented with 1 μg/ml puromycin (Sigma #P8833). Multiplicity of Infection (MOI) was calculated by counting the remaining cells 3 days after the start of selection.

MuSC lentiviral transduction and selection

Cells were seeded at 3,000 cells per cm^2 in 6-well plates in growth medium and 6 h later, medium was replaced by growth medium supplemented with 6 μg/ml polybren and lentivirus to a final MOI of 1. After 36 h, medium was replaced by selection medium (growth medium containing 1 μg/ml puromycin). After 3 days of puromycin selection, MuSCs were cultured in growth medium for 5-10 divisions for further analysis. Transduction efficacy was validated by IF for HA using anti-HA antibodies (1:200, Roche, 11583816001) according to the IF protocol described above.

Clonal cell culture

After LV-Myf5Promoter-GFP lentivirus transduction, cells were labeled with APC-conjugated anti-CD56 antibodies. Cells were sorted using a BD FACSAria II for $GFP^{pos}/CD56^{pos}$ cells, that were clonally seeded at one cell per well in 96-well plates coated with Matrigel (Corning Life Sciences) (Matrigel:conditioned growth medium [1v:99v]). Conditioned growth medium was recovered every 24h from healthy immortalized MuSCs.[35] Clones were cultured in conditioned medium until they reach the density of 3,000 cells per cm^2 and were thereafter cultured in growth medium for 4-6 weeks. Cells were proceeded for IF as described above using anti-CD56 mouse antibodies (1:10, Coulter #PN4235479-G) and anti-TCF7L2 rabbit antibodies (1:100, Cell Signaling Technology #C48H11), revealed by Cy3-coupled anti-mouse IgGs and Cy5-coupled anti-rabbit IgGs.

Quantitative RT-PCR

Total RNAs were extracted using NucleoSpin® RNA Plus XS kit (Macherey-Nagel #740990.50). The quality of RNA was checked using Nanodrop. One microgram of total RNA was reverse-transcripted using Superscript II Reverse Transcriptase (ThermoFisher #18064022) and diluted 5 times. Each sample was tested in triplicate. Quantitative RT-PCR was performed using CFX96 Real-Time PCR Detection System (Bio Rad). The 10 μl final volume of reactive mixture contained 2 μl of diluted cDNA, 0.5 μl of primer mixture (Table S5), 2.5 μl of water and 5 μl of LightCycler 480 SYBR Green I Master Kit (LifeSciences #04707518001). After initial denaturation of 2 min, the amplification was performed for 45 cycles of 95°C for 10 sec, 60°C for 5 sec and 72°C for 10 sec. The calculation of normalized relative quantity (NRQ) was performed using *AP3D1* or *B2M* as housekeeping genes for primers with annealing temperature at 60°C.[82]

Transcriptomic analysis

Total RNAs were extracted using NucleoSpin RNA Plus XS kit. RNA quality control was performed using Agilent 2100 Bioanalyser. Global gene expression was obtained using an Affymetrix GeneChip Human 8X60K chip. Data were normalized using LIMMA and controlled by principal component analysis before to compare the conditions with one-way ANOVA. Enrichment analysis was performed with DAVID gene ontology software. The transcriptome data are deposited at GEO as GSE229968.

Generation of a library for ATAC-seq

The ATAC-seq libraries were generated using 50,000 cells from two technical replicates of 1 DMD sample. The samples were used as detailed in.[83] In brief, nuclei were isolated and were incubated with a transposase solution (with a final concentration of transposase buffer 1X, 100 nM of transposase, 0.01% of digitonin, 0.1% of Tween-20 and PBS 0.33X) and incubated in a thermomixer with shaking at 1000 rpm for 30 min at 37°C. The mixture was cleaned using DNA Clean & Concentrator-TM-5 kit (Zymo #D4003). Next, transpose DNA was amplified by 12 cycles of PCR using SureSelectQXT Library Prep for WGS (Agilent #9684). The library quality and fragment size were quantified using an Agilent bioanalyzer 2100 before to be sequenced on Illumina HiSeq 4000 platform with paired-end sequencing. The ATACseq data are deposited at GEO as GSE232667.

ATAC-seq data processing

The adapter sequences were trimmed using Cutadapt 2.6. Next, the reads were aligned to the reference hg38 genome using Bowtie 2 v2.3.4.1. The files were sorted and indexed with Samtools v1.10 and mitochondrial reads were removed. Peak calling was performed using MACS2 2.1.2 with the default q-value cut-off of 0.05 and keep-dup 1. Functional annotation of peaks was done with ChIPseeker 3.1.1.

CUT&Tag

CUT&Tag was performed with mouse anti-HA antibodies (1:100, Genscript #A01244), rabbit anti-H3K4me3 antibodies (1:100, Sigma #04-745) or mouse anti-IgGs antibodies (1:100, Abcam #ab6708) using 7,500 cells as previously published.[84] In brief, after washes the cells were incubated with concanavalin A coated magnetic beads (Bangs Laboratories #BP531) for 15 min at RT. Bead-bound cells were incubated with the primary antibodies overnight at 4°C on a rotating platform. Primary antibodies were removed and mouse anti-IgGs antibodies (1:100, Abcam #ab6708) or rabbit anti-IgGs antibodies (1:100, Abcam #ab6708) were added for each condition and incubated for 1 h at RT. The cells were next incubated for 1 h at RT with pA-Tn5 adapter complex diluted at 1:250 before to proceed to the tagmentation for 1 h at 37°C. The tagmentation was stopped by an overnight incubation at 37°C after addition of 18 μl of a solution composed of 0.5 M EDTA, 10% SDS and 10 mg/ml proteinase K. A phenol:chloroform:isoamyl DNA isolation was performed.

Generation of the CUT&Tag library

To prepare libraries, 21 μl of DNA was mixed with 2 μl of universal i5 and i7 primers[85] and 25 μl of NEBNext HiFi 2X PCR master mix (NEB #M0544). Samples were amplified in a thermocycler as follows: 72°C for 5 min, 98°C for 30 sec, 14 cycles of 98°C for 10 sec and 63°C for 30 sec and a final extension at 72°C for 5 min. Post PCR clean-up was performed with GeneJET PCR Purification kit (Thermo Scientific #K0701).

Quantitative RT-PCR of CUT&Tag library

The promoter and enhancer of *mef2b* were defined from data of the human ENCODE project. The promoter was described at the TSS proposed by the human ENCODE project. The enhancer was identified by H3K4me marks downstream of the *mef2b* locus and associated with *mef2b* promoter by an Hi-C loop. Each sample was tested in triplicate. Quantitative PCR was performed on CUT&RUN libraries using CFX96 Real-Time PCR Detection System (Bio Rad). The 10 μl final volume of reactive mixture contained 2 μl of diluted cDNA, 0.5 μl of CUT&TAG primer mixture (Table S5), 2.5 μl of water and 5 μl of LightCycler 480 SYBR Green I Master Kit (LifeSciences #04707518001). After initial denaturation of 2 min, the amplification was performed for 45 cycles of 95°C for 10 sec, 60°C for 5 sec and 72°C for 10 sec.[82] The calculation of normalized relative quantity (NRQ) was performed by comparison of H3K9me3 and HA CUT&TAG samples to the IgG control samples.

QUANTIFICATION AND STATISTICAL ANALYSIS

All experiments were performed using at least 3 different donors (number of samples is given in the figure legends). Results are expressed using mean ± SEM. Statistics were performed using paired or unpaired t-tests or ANOVA and are given in the figure legends.